Journal of Hazardous Materials, Volume 381, January 2020, Article number 121200
DOI:10.1016/j.jhazmat.2019.121200

Environmentally friendly synthesized and magnetically recoverable designed ferrite photo-catalysts for wastewater treatment applications

Daphne Hermosilla[1], Changseok Han[2], Mallikarjuna Nadagouda[3], Libor Machala[4], Antonio Gascó[5], Pablo Campo[6], Dionysios D. Dionysiou[7]*

[1]*Department of Agricultural and Forestry Engineering, University of Valladolid, EIFAB, Campus Duques de Soria, 42004 Soria, Spain.*

[2]*Department of Environmental Engineering, INHA University, Incheon, 22212, Korea.*

[3]*Center for Nanoscale Multifunctional Materials, Mechanical & Material Engineering, Wright State University, Dayton, OH 45431, USA.*

[4]*Regional Centre of Advanced Technologies and Materials, Department of Experimental Physics, Faculty of Science, Palacký University, Šlechtitelů 27, 783 71 Olomouc, Czech Republic.*

[5]*Department of Agricultural and Forest Sciences, University of Valladolid, EIFAB, Campus Duques de Soria, 42004 Soria, Spain.*

[6]*Cranfield Water Science Institute, Cranfield University, Cranfield MK43 0AL, UK*

[7]*Environmental Engineering and Science Program, Department of Chemical and Environmental Engineering, University of Cincinnati, Cincinnati, OH 45221-0012, USA.*

[*] Corresponding author:
Tel.: +34 9759471, e-mail: daphne.hermosilla@uva.es

Declarations of interest: none.

Abstract

Fenton processes are promising wastewater treatment alternatives for bio-recalcitrant compounds. Three different methods (i.e., reverse microemulsion, sol-gel, and combustion) were designed to synthesize environmentally friendly ferrites as magnetically recoverable catalysts to be applied for the decomposition of two pharmaceuticals (ciprofloxacin and carbamazepine) that are frequently detected in water bodies. The catalysts were used in a heterogeneous solar photo-Fenton treatment to save the cost of applying high-energy UV radiation sources, and was performed under a slightly basic pH to avoid metal leaching and adding salts for pH adjustment. All the developed catalysts resulted in the effective treatment of ciprofloxacin and carbamazepine in both synthetic and real domestic wastewater. In particular, the sol-gel synthesized ferrite was more magnetic and more suitable for reuse. The degradation pathways of both compounds were elucidated for this treatment. The degradation of ciprofloxacin involved attacks to the quinolone and piperazine rings. The degradation pathway of carbamazepine involved the formation of hydroxyl carbamazepine and dihydroxy carbamazepine before yielding acridine by hydrogen abstraction, decarboxylation, and amine cleavage, which would be further oxidized.

Keywords

Advanced Oxidation Processes, Ferrites, Photo-Fenton, Ciprofloxacin, Carbamazepine.

Published by Elsevier. This is the Author Accepted Manuscript issued with: Creative Commons Attribution Non-Commercial No Derivatives License (CC:BY:NC:ND 4.0).
The final published version (version of record) is available online at DOI:10.1016/j.jhazmat.2019.121200. Please refer to any applicable publisher terms of use.

1. Introduction

The total retail pharmaceutical bill in OECD countries amounted to approximately 800 billion USD in 2013 (OECD, 2015). Pharmaceuticals are consumed by humans or animals and partially metabolized and excreted through sewers or garbage, further entering into the environment through landfills, the outflow of wastewater treatment plant (WWTP) effluents, in association with biosolids, or being directly discharged. It is therefore becoming an environmental issue of great concern (Hao et al., 2007; Mohapatra et al., 2014).

Most WWTPs are not devised to remove bio-recalcitrant substances; thus, many pharmaceuticals are continuously being discharged into receiving water bodies (Bobu et al., 2008; Wang et al., 2018a). As their efficiency to eliminate bio-recalcitrant compounds in wastewater has already been proved (Barndõk et al., 2016; Hermosilla et al., 2012), advanced oxidation processes (AOPs) are a potential good treatment alternative for them. Nevertheless, their full application is limited by their high-energy consumption and the potential generation of toxic byproducts. These drawbacks could be overcome by implementing alternative treatment strategies, such as the development of new photo-catalytic technologies, the wise integration of AOPs with other treatment processes (e.g. biological) (Barndõk et al., 2013; Barndõk et al., 2016; Merayo et al., 2013a), or the combination of both.

Photocatalysis is a well-recognized process for the treatment of bio-recalcitrant organic compounds that has demonstrated higher efficiency, better sustainability, easier operation, and lower cost than conventional technologies and some other AOPs for the removal of antibiotics under certain conditions, particularly when using solar energy (Barndõk et al., 2013; Fiorentino et al., 2019: Jiang et al., 2017; Yuan et al., 2017). The development of highly efficient catalysts in general terms, or specifically those working within the visible light range or the solar spectrum, which are more economical and less harmful to use, is key for the improvement of photocatalytic environmental applications.

Examples of such catalysts include TiO_2-based semiconductor materials (Barndõk et al., 2013; Wang et al., 2018b; Wang et al., 2019), some carbon-based materials (Wang et al., 2018a; K. Zhang et al., 2016; S. Zhang et al., 2016), perovskite-based catalysts (Wu et al., 2018), or metals (Blanco et al., 2016; Dias et al., 2016; Du et al., 2016; Sharma and Singhal 2015; Zhang and Huang, 2005), among others.

In particular, ferrites (MFe_2O_4, M = divalent cation) are promising materials that could be useful to develop heterogeneous photo-Fenton processes. Fenton processes are environmentally and economically friendly treatment alternatives that have proven their efficacy in treating bio-recalcitrant compounds in wastewater (Hermosilla et al., 2012; Hermosilla et al., 2015). Nevertheless, the actual industrial application of Fenton processes is limited by the need to apply acidic pH conditions to achieve a high efficiency (Hermosilla et al., 2012), and the production of undesirable metal sludge along treatment. This drawback could, however, be much reduced by the application of UV-radiation in photo-assisted Fenton processes (Hermosilla et al., 2009a, 2009b, 2012), which results in such processes being more economical, sustainable, and feasible when using solar radiation. Besides, the solar photo-Fenton treatment is more competitive if metal sludge production could further be attenuated or even totally avoided by keeping the pH of wastewater close to neutral without the need to add acids (Rodríguez et al., 2016).

In addition, the use of ferrites prevents metal sludge production and enables easier catalyst recovery and reuse thanks to their magnetic properties (Sharma and Singhal, 2015). Moreover, ferrites are chemically and thermally stable (Yang et al., 2013), and their quite narrow active band makes them effective catalysts under visible radiation (Wang et al., 2011).

Several studies have already reported different alternatives to avoid disadvantageous iron sludge production by: (a) recovering the sludge (Kishimoto et al., 2013); (b) preparing

recoverable iron catalysts, namely: Fe^0 (Barndõk et al., 2016), iron-coated pumice particles (Alver et al., 2016), iron alginate (Ben Hammouda et al., 2016), waste rich in iron oxide (Dias et al., 2016), magnetic nanoparticles supported in titanate nanotubes (Du et al., 2016), carbon nanofiber support for iron oxide (Lubej et al., 2016), or nanocomposites (M. Wang et al., 2016); (c) combining the process with electricity (electro-Fenton) (Moreira et al., 2017); (d) applying UV-light (photo-Fenton (Hermosilla et al., 2009a, 2009b); or (e) designing Fenton-like systems by using different metal catalysts (Bokare and Choi, 2014; Sharma and Singhal, 2015).

Some environmental applications have already been addressed for the use of ferrite catalysts. For example, they were successfully applied in the degradation of several dyes, such as using $BiFeO_3$ and $NiFe_2O_4$ nanoparticles to efficiently remove Rhodamine B (Wang et al., 2011; An et al., 2013). Furthermore, Mahmoodi (2013) reported the degradation of Reactive Reds 120 and 198 using magnetic zinc-ferrite nanoparticles, concluding that H_2O_2 addition was necessary for an effective treatment; whereas Sharma and Singhal (2015) applied spinel ferrites (MFe_2O_4; M = Zn, Cu, Ni or Co) to degrade reactive azo dye RB5 by Fenton and photo-Fenton processes, reporting significantly improved reaction rates in light-assisted treatment. Furthermore, Cu-ferrites showed a higher activity owing to higher hydroxyl radical productions thanks to Cu^{2+} participation in Fenton's reaction. Besides, Guan et al. (2013) synthesized magnetic $CuFe_2O_4$ to catalyze the oxidation of atrazine herbicide.

Carbamazepine is an analgesic, anticonvulsant, and antimanic agent that has been reported to be the most frequent pharmaceutical present in natural water resources (Zhang et al., 2008); that is, carbamazepine and its metabolites are continuously being released into the environment affecting water quality (Mohapatra et al., 2012). In addition, fluoroquinolones (ciprofloxacin particularly) are nowadays one of the major prescribed types of antibiotics (Bobu et al., 2008; Dodd et al., 2005). Unfortunately, the occurrence of fluoroquinolones and

their degradation byproducts in water bodies has also been reported in several countries (Switzerland, USA, and Australia) (An et al., 2010; Ikehata et al., 2008; Watkinson et al., 2007; Zhang and Huang, 2005). The worldwide presence of these pharmaceuticals in natural water resources denotes the aforementioned limitation of conventional wastewater treatment technologies to remove them. In fact, the content of a wide range of antibiotics in water bodies can pose severe threats to human health and the ecosystems even at low concentrations because of their toxicity and the induction of antibiotic resistance (An et al., 2010; Zhu et al., 2016).

The central objective of this research was to develop new environmentally-friendly synthesized magnetically-recoverable ferrite catalysts for the treatment of emerging bio-recalcitrant contaminants such as carbamazepine and ciprofloxacin. These iron-based catalysts were prepared by modifying conventional preparation methods to turn them into more environmentally-friendly processes. The catalytic efficiency of the newly synthesized ferrites was tested by the solar photo-Fenton treatment of ciprofloxacin and carbamazepine in aqueous synthetic solutions and in treated domestic wastewater.

2. Material and methods

2.1. Material

Analytical-grade chemicals (Merck KGaA, Darmstadt, Germany; and Sigma Aldrich, Missouri, USA) were used without further purification. The physicochemical characterization of carbamazepine and ciprofloxacin is shown in Table 1.

Biologically-treated domestic wastewater (Table 2) was collected from a pilot membrane bioreactor at the University of Cincinnati (Ohio, USA). The initial contents of ciprofloxacin and carbamazepine were 10 $\mu g\ L^{-1}$

Synthetic water samples were prepared by adding ciprofloxacin and carbamazepine (TOC ≈ 5 mg L^{-1}) to Type 1 ultrapure water (Mili-Q, Merck Millipore). The alkalinity of the wastewater was 135 mg L^{-1} of $CaCO_3$ (Table 2). $Ca(OH)_2$ was added to simulate the same alkalinity and initial pH value of this wastewater (pH ≈ 8) and buffer it along treatment.

2.2. Ferrite synthesis

Reverse microemulsion, sol-gel, and combustion methods were developed to synthesize $MnFe_2O_4$ and Fe_3O_4 ferrites in an environmentally-friendly way. Various addressed-as-optimal conditions were assessed according to the literature (Flanagan et al., 2006; Goldman, 2006; Hashim et al., 2015; Mendonca et al., 2009; Sharma and Singhal, 2015) and our previous experience before the herein described preparation methodologies were postulated as optimal to perform our experiments.

The reverse microemulsion method was modified from the protocol described in Hashim et al. (2015) by substituting several chemicals of its formula based on other microemulsion preparation methods (Flanagan et al., 2006; Mendonca et al., 2009) to synthesize ferrites in a more environmentally-friendly way. Cyclohexane oil was replaced by soy oil. Methyl-ammonium bromide (CTAB) was substituted by Agnique PG 8105 (Cognis, USA), which is a readily-biodegradable Br-free non-ionic surfactant entirely based on renewable raw materials. Isoamyl alcohol was replaced by ethylene glycol as co-surfactant. Manganese acetylacetone [$(C_5H_8O_2)_2Mn$] and ferric nitrate nonahydrate ($FeN_3O_9{\cdot}9H_2O$) were used as metal precursors. The emulsions were sonicated until getting clear solutions. Two microemulsions were initially prepared to synthesize the desired ferrite. First, mixing stoichiometric amounts of $(C_5H_8O_2)_2Mn$ and $FeN_3O_9{\cdot}9H_2O$ in a 1:2 molar ratio, then adding soy oil, surfactant, and cosurfactant in 1:1 weight ratios to total metals content, and finally adding water in a 10:12 weight ratio to soy oil content. Secondly, a reverse microemulsion was similarly prepared with 0.1 M NaOH as aqueous phase. Both solutions were quickly

mixed under vigorous stirring at a constant T = 80 ºC. To complete the reaction, the resulting mixed solution was kept at pH = 9 while being stirred for 2 h. An equal volume of isopropanol and acetone was then supplemented to the solution, which was centrifuged to separate the solid product. This collected solid was washed with water and acetone, and oven-dried for 24 h at T = 100 ºC. Samples were annealed for 4 h at 700 ^{o}C with a heating ramp-rate of 10 ºC min^{-1}. The resulting ferrite particles were obtained in powder form.

The sol-gel method was developed as a modification of other preparation protocols (Sharma and Singhal, 2015; Goldman 2006). The metal precursors $(C_5H_8O_2)_2Mn$ and $FeN_3O_9{\cdot}9H_2O$ were used in a 1:2 molar proportion. The required amounts of metals were dissolved in a minimum volume of distilled water, and the resulting solution was heated at 90 ^{o}C for 2 h. After the formation of a homogeneous solution, ethylene glycol and citric acid were added in a 1:1 weight ratio to metal content. This solution was stirred until the gel was formed, then aged for 24 h, and subsequently dried at 120 ºC for 1 h to obtain ferrite powder, which was annealed for 4 h at 500 ^{o}C with a heating ramp-rate of 10 ºC min^{-1}.

To apply the combustion method, $(C_5H_8O_2)_2Mn$ and $FeN_3O_9{\cdot}9H_2O$ were mixed in a 1:2 Mn:Fe molar ratio by adding cellulose in a 1:1.5 metals:cellulose weight ratio. This blend was thereafter heated at 400 °C in a furnace for 30 min. To investigate the effect of cellulose on the synthesis of ferrite, this method was also performed without cellulose addition.

To compare $MnFe_2O_4$ and Fe_3O_4 ferrites behavior, control ferrites were also prepared by these three methodologies just using $FeN_3O_9{\cdot}9H_2O$.

2.3. Characterization of ferrites

The crystallographic structure of each ferrite was identified by X-ray diffractometry (XRD) following the Grazing incident method in a Philips X'pert pro MRD instrument. A parabolic mirror was used in the primary optic. A parallel plate collimator with a secondary

monochromator was used in the secondary optic. The applied radiation was Cu Kα (λ = 1.54Å).

The Brunauer–Emmett–Teller (BET) surface area, pore volume, porosity, Barret–Joyner–Halenda (BJH) pore size and distribution were measured with an ASAP 2020 physisorption analyzer (Micromeritics, Norcross, USA). Samples were previously purged for 2 h with N_2 at T = 150 °C.

The morphology of the material was characterized by a JSM-6490LV scanning electron microscope (SEM, JEOL). Films were coated with carbon for this purpose.

Detailed information of the crystal size and structure at the nanoscale was obtained by transmission electron microscopy (TEM) with a JEM 2010F microscope (0.17 nm point resolution). Samples were ultrasonically dispersed in butanol (99.5 %, Panreac, Spain), and then laid on a holey carbon-film covered copper grid before TEM analysis.

Magnetic properties were determined on powder samples with a "*Quantum Design Physical Properties Measurement System*" (PPMS Dynacool system) incorporating the VSM option. Results were corrected for the diamagnetism and signal produced by the sample holder. Hysteresis loops were registered at T = 300 K in external magnetic fields ranging from −9 to +9T. A zero-field Mössbauer experiment at room temperature was carried out with a transmission Mössbauer spectrometer MS96 with a ^{57}Co(Rh) source of γ–rays. Mössbauer spectra were fitted to Lorentzian line shapes based on the least-square method using the program MossWinn. Isomer shift values were referred to α–Fe foil samples at room temperature.

2.4. Photocatalytic treatment

The photocatalytic degradation of ciprofloxacin and carbamazepine was performed by solar photo-Fenton treatment in a glass reactor (11.5 cm i.d.; V = 250 mL) covered with a quartz lid and sealed with parafilm. A 500 W solar simulator (Newport Corporation, Irvine, USA)

equipped with air mass (AM 1.5) and infrared filters were used for illumination. 70 W cm^{-2} of light intensity were measured by a radiant-power meter (Newport Corporation, Irvine, USA).

Wastewater (100 mL) was first poured into the reactor. Then, the ferrite catalyst was added. Finally, the corresponding H_2O_2 dosage was incorporated in batch mode (reaction time=0) when light radiation stabilized at 500 W. Samples were withdrawn at designed time gaps and filtered using 0.45 µm PVDF syringe filters to measure pH and the concentrations of H_2O_2, Mn, Fe, target compounds, and their byproducts.

No measurable adsorption of the contaminants on the catalyst was found in dark adsorption tests. The following wastewater treatment control trials were performed: (a) just in the dark; (b) adding the catalyst standalone with and without photo-assistance; and (c) adding H_2O_2 without the catalyst but applying solar-radiation.

Different concentration ratios of $[H_2O_2]/[COD]$ (in mg L^{-1}) and $[H_2O_2]/[Fe^{2+}]$ (molar) were tested to optimize treatment. $[H_2O_2]/[COD] = 2.125$ was selected as optimal for Fenton treatment (Hermosilla et al., 2009b; Merayo et al., 2013b); and $[H_2O_2]/[COD] = 4.250$ was also investigated as previously reported as the optimal for degrading ciprofloxacin and carbamazepine (Bobu et al., 2008). $[H_2O_2]/[Fe, Mn]$ molar ratios of 1, 2, 5, and 10 were assessed. All experiments were performed in triplicate.

Ciprofloxacin and carbamazepine were separately treated in synthetic water ([TOC] = 5 mg L^{-1}) to investigate the generation of transformation products (TPs) and their individual response to treatment. Both compounds were also treated together in the aforementioned biologically-treated domestic wastewater.

2.5. Analytical methods

All chemical analyses were performed according to the "*Standard Methods for the Examination of Water and Wastewater*" (APHA et al., 2016). pH was measured with a pH-electrode and alkalinity was estimated by titration with 0.1 N H_2SO_4. H_2O_2 content was

determined by the titanium sulfate spectrophotometric method (Hermosilla et al., 2009a, 2009b). Total Fe and Mn were measured with an Agilent (Palo Alto, CA, USA) 7700 series ICP-MS. Turbidity was measured with a Hanna Instruments LP2000-11 turbidity meter (Woonsocket, RI, USA).

The concentration of antibiotics was determined by an Agilent 1100 HPLC (Palo Alto, CA, USA). When measuring the presence of carbamazepine, the mobile phase was composed of water (A) and methanol (B) in a 50:50 v/v proportion, and the eluate was monitored at 285 nm. For ciprofloxacin, the mobile phase consisted of 0.02 M H_3PO_4 and acetonitrile in an 85 to 15 % proportion (v/v), and the detection wavelength was 280 nm. In both cases, separation was achieved with a C18 column at ambient temperature, and the mobile phase flow-rate was 1 mL min^{-1}.

Trace concentrations of carbamazepine and ciprofloxacin in treated domestic wastewater samples were analyzed with a 1200 series LC and a 6410A triple MS/MS equipped with an electrospray ionization source from Agilent (Palo Alto, CA, USA). The pharmaceuticals were separated with a Zorbax Eclipse XDB-C18 column (2.1×50 mm, 3.5 µm) from Agilent. The flow-rate was 0.2 mL min^{-1}. The mobile phase was composed of water (A) and acetonitrile (B), both containing a 0.1 % of formic acid. The eluent composition was 95 % (A) at time = 0, decreasing to 5 % after 6 min. The column required a 2 min post-run stage to equilibrate. The injection volume was 10 µL. The electrospray was operated in positive mode under the following conditions: nebulizer = 40 psig, drying gas flow = 9 L min^{-1}, drying gas temperature = 300 °C, fragmentor = 110 V, and capillary = 3,500 V.

The pharmaceuticals were detected by monitoring the selected fragmentation reactions *m/z* 237 → *m/z* 194 for carbamazepine, and *m/z* 332 → *m/z* 314 for ciprofloxacin. The respective collision energies for carbamazepine and ciprofloxacin were 15 and 20 V.

Ciprofloxacin and carbamazepine TPs were identified performing accurate mass experiments with a 1290LC system connected to a 6540 accurate-mass quadrupole time-of-flight mass spectrometer (Q-TOF) from Agilent (Palo Alto, CA, USA). Chromatography conditions were similar to those described for MS/MS experiments. Ionization was realized by a jet stream electrospray operated in positive ion mode under the following conditions: sheath gas temperature = 250 °C, nebulizer = 45 psig, gas flow = 7 L min^{-1}; gas temperature = 350 °C, skimmer = 45 V, fragmentor = 150 V, nozzle = 0 V, octopole RF = 750 V, and capillary = 3,500 V. Accurate mass spectra were obtained in scan mode (50-1200 *m/z*). Reference masses were 121.0509 and 922.0098 *m/z* with a resolution of 19,546 at 922.0106 *m/z*. High-resolution spectra were processed with Agilent's MassHunter software (version B.07.00). Considering ciprofloxacin and carbamazepine as parent compounds, the corresponding TPs were identified by applying mass defect filters of 0.1332 ± 0.05 and 0.095 ± 0.05 Da, respectively.

3. Results and discussion

3.1. Morphology and microstructure of ferrites

Figure 1 shows SEM images of the synthesized ferrite samples. By combustion and sol-gel processes, quite small particles (< 50 nm) were synthesized. The shape and size of particles were effectively controlled in the sol-gel process, which led to the formation of spherical particles < 25 nm. By the reverse microemulsion method, particles > 100 nm were produced and, especially, rod-type shapes were generated when Mn-ferrites were formed.

The combustion process produced ferrites with high surface area and a higher proportion of Mn to Fe content in comparison with those synthesized by the other methods (Tables 3 and 4). The sol-gel process resulted in ferrites with a relatively high surface area, high crystallinity, and a similar content of both metals, although Fe content was higher. In

contrast, ferrites synthesized by reverse-microemulsion showed a lower surface area, but a higher Fe content. Summarizing, sol-gel and combustion methods produced higher surface area ferrites, probably because of their higher Mn content. The presence of cellulose reduced the surface area of ferrites produced by combustion (Table 3).

Figure 2 shows TEM and HR-TEM images of the synthesized $MnFe_2O_4$ samples. Particles of 10-100 nm were synthesized forming aggregates. The measured lattice spacing of 0.29 nm corresponded to the (220) crystallographic plane of $MnFe_2O_4$ (Kim et al., 2010) and confirmed the production of Mn-ferrites by the combustion. In contrast to the other two methods, larger and more spherical particles were formed by reverse microemulsion. Particle size ranged from 30 to 200 nm, which corroborated SEM observation results. The measured lattice spacing was 0.48 nm, which corresponds to the (111) plane of $MnFe_2O_4$ (Desai, 2013). This indicates that Mn-ferrites were also successfully produced by reverse microemulsion. Aggregates of different sized nanoparticles (5-200 nm) were observed in sol-gel samples The lattice spacing of the sample resulted in 0.29 nm as well, which corresponds to the (220) plane of $MnFe_2O_4$ (Kim et al., 2010); therefore confirming that Mn-ferrites were also effectively prepared by the sol-gel method.

Figure 3 shows XRD patterns of synthesized $MnFe_2O_4$ and control ferrite. All peaks corresponding to hematite (α-Fe_2O_3) were found by XRD analysis, indicating that control Fe_3O_4 was non-magnetic (JCPDF 11-001-1053). Reverse microemulsion mainly produced $MnFe_2O_4$ containing hematite as well, although a small peak corresponding to the (311) plane of $MnFe_2O_4$ (JCPDF 00-038-0430) was also found. Combustion and sol-gel Mn-ferrites were mainly a mix of hematite and $MnFe_2O_4$, and showed strong magnetic properties. In fact, small peaks corresponding to the (311), (511), and (440) planes of magnetite Fe_3O_4 were observed (JCPDF 01-075-0449), which explains their stronger magnetic properties in comparison with control Fe_3O_4 and reverse microemulsion $MnFe_2O_4$.

The XPS analysis of sol-gel $MnFe_2O_4$ showed main peaks due to Fe 2p, Mn 2p, O 1s, and C 1s. The O 1s peak was produced at about 530 eV and has been assigned to contributions from Mn-O, C–O, Fe-O, O-H, and C-OH groups (Wan et al., 2014). The Fe 2p doublets with binding energy values of 710 and 725 eV indicate the presence of Fe-O bonds, which furthermore denotes Fe oxidation on the surface of the ferrite (Wan et al., 2014). The Mn 2p spectrum observed at 641 eV indicates the presence of Mn-O bonds. The synthesized magnetic metal oxides were likely to occur as a mixture of Fe 2p and Mn 2p with oxygen, which further proves the presence of $MnFe_2O_4$ nano-crystals. The analysis of the combustion-synthesized $MnFe_2O_4$ ferrite showed a similar pattern, also denoting $MnFe_2O_4$ nanocrystals presence (Figure 4).

3.2. Magnetization

Magnetism is a critical property determining the more suitable material for its environmental application as a catalyst. Magnetization is strongly influenced by the relative content of α-Fe_2O_3 because this polymorph behaves as a weak ferromagnet at room temperature and has a negligible contribution to net magnetization. Thus, sol-gel synthesized Fe_3O_4, reverse microemulsion $MnFe_2O_4$ and Fe_3O_4, and combustion-generated Fe_3O_4 showed very low magnetization (from 1.7 to 3.7 emu g^{-1}; Table 5) due to their major α-Fe_2O_3 contents.

Superparamagnetism is determined by particle size, and the presence of superparamagnetic nanoparticles reduces net magnetization. Table 5 shows relative contents of superparamagnetic phase (SP) and α-Fe_2O_3, as determined from Mössbauer spectra (Figure SI1). Although the effect is not so considerable as in the case of α-Fe_2O_3 content, superparamagnetism explains the shown magnetization differences between sol-gel and combustion synthesized Mn-ferrites (Table 5; Figure 5). The macroscopic magnetic behavior of the samples was easily visualized using a magnet (Figure 5).

Magnetization values of sol-gel $MnFe_2O_4$ were higher than those reported elsewhere

(Wan et al., 2014), yet within the lower range of previously reported results for $MnFe_2O_4$ nanoparticles (Masala and Seshadri, 2005). Reverse-microemulsion synthesized Mn-ferrite showed the lowest values of magnetization, as previously reported for reverse micelles and co-precipitation procedures (Masala and Seshadri, 2005). This could be due to the magnetic disorder associated with the absence of crystallinity of the nanoparticles, as well as to different levels of cation vacancy disorder. It has also previously been reported that $MnFe_2O_4$ nanoparticles produced by co-precipitation or reverse micelle methods can show core and surface defects (Masala and Seshadri, 2005).

3.3. The treatment of wastewater

Although different $[H_2O_2]$/COD ratios were tested to optimize treatment, the theoretical stoichiometric dosage to achieve the complete oxidation of the COD is 2.125 g of H_2O_2 per 1 g of COD (Kim et al., 1997), which is within the optimum values (2.00-2.40) reported to maximize COD removal in the Fenton treatment of highly organic-loaded stabilized landfill leachate (Hermosilla et al., 2009b), brines (Rivas et al., 2003), and phenol (Kavitha and Palanivelu, 2004). The best treatment of ciprofloxacin at $[H_2O_2]$/COD = 2.125 achieved a maximum 60 % removal of this antibiotic in treated domestic wastewater and the 80 % in synthetic water once all H_2O_2 was consumed. When $[H_2O_2]$/COD was raised up to 4.250 to maximize the removal of both antibiotics, as reported by Bobu et al. (2008), these treatment results enhanced up to an 80 % and over the 95 %, respectively (Figures 6 and 7).

These removal results were similar to those reported by other authors for the photo-Fenton treatment of ciprofloxacin under neutral or basic pH values, such as Bobu et al. (2008), who used modified laponite clay-based Fe nanocomposite (Fe-Lap-RD) as a heterogeneous catalyst in the process; but we used about four times lower H_2O_2 to ciprofloxacin concentration ratio. In addition, the ciprofloxacin removal results obtained in our study were also comparable to, or even better than those reported using magnetite

nanoparticles as magnetic catalyst and performing the treatment at the initial natural pH value of the solution (Lima et al., 2014); as well as than when the treatment was performed at a maximum pH value of 4.5 adding other iron sources (iron citrate, oxalate, and nitrate) to catalyze the photo-assisted Fenton reaction (Lima Perini et al., 2013). As expected (Blanco et al., 2016; Hermosilla et al., 2009b), faster kinetics were produced when the photo-Fenton treatment was performed at an acidic pH value, or when higher H_2O_2 doses and lower $[H_2O_2]$/[Fe] ratios were used.

The reduction of the $[H_2O_2]$/[Fe, Mn] molar ratio to perform the treatment at a fixed optimum $[H_2O_2]$ increases the kinetics of both H_2O_2 decomposition and contaminants removal. For example, the rate constants for H_2O_2 decomposition were 10-fold higher at a 1:1 molar ratio (k = 0.039, r^2 = 0.99) than at 10:1 (k = 0.0036, r^2 = 0.98) for the sol-gel synthesized catalyst. Although iron sludge generation would also result progressively reduced at higher $[H_2O_2]$/[Fe, Mn], the required treatment time would also increase much. Thus, $[H_2O_2]$/[Fe, Mn]=5 was finally used to test all the synthesized ferrites to properly follow the kinetics and the generation of TPs along the process.

The advantage of working with heterogeneous catalysts is that there is no ferric hydroxides generation at basic pH values; hence, better efficiencies were achieved at pH > 8 when the synthetized ferrites were used as catalysts than with other materials (Giri and Golder, 2019). Furthermore, the achieved treatment efficiency was similar, or even higher than the reported for conventional titania-based treatments (Giri and Golder, 2019); as well as similar to other improved catalysts, such as $W_{18}O_{49}$/g-C_3N_4 nanograss composites, which achieved over the 90 % removal of ciprofloxacin after 120 min of photocatalytic treatment (Deng et al., 2018).

Carbamazepine was removed up to a 20-25 % in treated domestic wastewater (Figure 7) and about a 35-40 % in synthetic water at its best (Figure 8). These results match those

reported for the treatment of groundwater by the UVA/FeIII-NTA/$S_2O_8^{2-}$ process (Jin et al., 2019), and for the modified photo-Fenton treatment of tertiary effluents designed by Klamerth et al. (2012). On the other hand, these carbamazepine removal efficiencies are lower, and the degradation kinetics are slower, than those reported for the photo-Fenton treatment of carbamazepine-containing synthetic water performed at acidic pH values because of the use of a heterogeneous catalyst, the constant basic pH value, and the significant concentration of bicarbonate required to keep a basic pH solution, which slows down the oxidation kinetics and scavenges part of the produced radicals (Barndõk et al., 2012). In particular, the reactivity of HO· with bicarbonate has been estimated to have a second order constant rate of 8.5 x 10^6 M^{-1} s^{-1} (Buxton et al., 1988). Nevertheless, our developed catalysts showed the advantage of achieving good efficiency results even at basic pH values and in the presence of salts.

Combustion-synthesized ferrites showed the worst treatment results (Figure 6) despite possessing the highest surface area (Table 3). The main cause for this may have been the observed increase of turbidity in the solution (54 NTU for the combustion-synthesized $MnFe_2O_4$ vs. 18 NTU of the sol-gel $MnFe_2O_4$), which surely hindered light transmittance. In addition, the different amount of iron present in its composition (Table 4), in contrast with ferrites produced by the other methods, can also partially explain these results.

The sol-gel synthetized $MnFe_2O_4$ showed better magnetic properties than the other ferrites (Figure 5), and higher surface area (Table 3) than the microemulsion synthetized one, despite its lower iron content (Table 4). Moreover, the sol-gel produced $MnFe_2O_4$ was the most efficient ferrite in the decomposition of H_2O_2 under solar irradiation. Interestingly, there was not any remaining hydrogen peroxide in the solution after 120 min of treatment at the higher tested level of H_2O_2 concentration; whereas about a 10 % was measured in the solution when the microemulsion $MnFe_2O_4$ was used, which could partially be attributed to

the higher surface area of sol-gel produced $MnFe_2O_4$ (Table 3). Furthermore, these catalysts were magnetically recoverable and yielded comparable removal efficiencies after 5 uses (Figure 9). No Fe-leaching was observed during treatment, probably due to the higher binding energy of Fe with respect to Mn. In fact, a slight Mn leaching (< 2 μg L^{-1}) was detected within consent values of European regulations for potable water (< 50 μg L^{-1}) (Council of the European Union, 1998).

Ciprofloxacin was almost totally removed (>95 %; Figure 6) and carbamazepine was reduced up to a 25 % (Figure 8) when using the sol-gel $MnFe_2O_4$. As shown in Figure 8, the presence of this catalyst more than doubled the degradation constant rate of carbamazepine after the addition of H_2O_2, namely: k = 0.0026 with catalyst, and k = 0.0011 without it; as well as it almost doubled that of ciprofloxacin, namely: k = 0.0216 with catalyst, and k = 0.0125 without catalyst (R^2 values > 0.95 in all the cases). The removal of both compounds in treated domestic wastewater followed a very similar trend to the treatment of synthetic wastewater using sol-gel synthesized $MnFe_2O_4$ (Figure 7); namely, ciprofloxacin was highly removed (≥ 80% after 4 to 8 h), and carbamazepine was degraded ≈ 25 % after 4 h, and almost reached the 60 % after 8 h.

No removal of contaminants was achieved under dark conditions (conventional Fenton process) since solar irradiation is required for ferrites to regenerate ferrous iron from the reduction of ferric iron to properly perform the Fenton reaction generating hydroxyl radical from the decomposition of hydrogen peroxide. The conventional Fenton treatment of ciprofloxacin has been reported as not being able to achieve such good removal results as its photo-assisted version (74.4 % in the best case reported) (Giri and Golder, 2014) because it is limited by the formation of ciprofloxacin-iron complexes and the need of an acidic pH environment to avoid the formation of iron hydroxides (Giri and Golder, 2019). No

adsorption of the contaminants was observed on the catalyst either. The reaction was always conducted at values close to pH = 8 thanks to the bicarbonate buffer action.

TPs resulting from the oxidation reaction were detected by accurate mass analysis, and degradation pathways could therefore be postulated. For ciprofloxacin, main TPs had mass values of 348.1344 (error -4.3 ppm) and 334.1191 (error -3.65 ppm), which coincide with previously found TPs (Zhu et al., 2016) corresponding to molecular formulas shown in Figure 10. A possible ciprofloxacin degradation route has previously been described based on the hydroxyl radical attack to the quinolone ring, which has the atom with the highest $FED^2_{HOMO}+2FED^2_{LUMO}$ value, being C5 and C10 the most reasonable sites for hydroxyl radicals addition (An et al., 2010). The A intermediate resulted from the hydroxyl radical attack to C5, and the B intermediate resulted from its attack to C10 (Figure 10).

Besides this pathway, the most probable route for ciprofloxacin degradation according to the performed mass analysis involved the breakdown of the piperazine ring via N-dealkylation and C-hydroxylations by addition of hydroxyl radicals to the aromatic ring (E to F and G route, Figure 10), which generates an anilinyl radical intermediate (Bobu et al., 2008; Zhang and Huang et al., 2005). TPs with masses values of 362.9646, 360.3605, and 263.0821 were also found in much less quantity along treatment.

The increasing peak areas observed in the chromatograms at different treatment times offered compelling evidence that ciprofloxacin degradation started with the addition of OH· to the above-described alternative positions forming 348 mass TPs, and oxidation progressed to 334 mass TPs (Figure 10). The abundance of 348 mass TPs remained more or less constant along treatment, and 334 mass TPs content was higher after 30 minutes of treatment, which began to decrease afterwards, being its concentration at 120 minutes ≈ 25 % lower than at 30 minutes. Alternatively, the 348 intermediate only appeared after 120 minutes of reaction when only H_2O_2 was used (without catalyst).

For carbamazepine, two compounds were also identified: (Figure 11): $C_{13}H_9N$ (mass 179.0733, error -1.37 ppm) and $C_{15}H_{12}N_2O_2$ (mass 252.0901, error 0.8 ppm). The formation of these can be linked to a first OH· mediated oxidation to hydroxy carbamazapine, and a posterior degradation to acridine. Similar results have been reported elsewhere (Nawaz et al., 2017; W.L. Wang et al., 2016; Yang et al., 2016). Carbamazepine is attacked by OH· radicals to produce monohydroxy carbamazepine. This TP may then incorporate another OH· radical forming dihydroxy carbamazepine (Nawaz et al., 2017), and its further degradation by amine cleavage, hydrogen abstraction, and decarboxylation finally produces acridine, which was detected in a high concentration. Its concentration after 2 h of treatment was double than after 1 h.

4. Conclusions

Magnetically recoverable ferrite catalysts were produced by the three proposed environmentally friendly modifications of the combustion, microemulsion, and sol-gel ferrite preparation methods. The sol-gel synthesized ferrite catalyst resulted in being more magnetic than the other two and could therefore be better reused for wastewater treatment.

Overall, the application of all the developed catalysts resulted in an effective treatment of ciprofloxacin and carbamazepine by the photo-Fenton process in both synthetic and actual treated domestic wastewater, although the use of sol-gel and microemulsion synthesized ferrite catalysts notably demonstrated higher treatment efficiencies than those produced by the combustion method.

The degradation routes of both compounds by the applied ferrite-catalyzed heterogeneous photo-Fenton treatment were postulated. The degradation route of ciprofloxacin progressed after the attacks to the quinolone and piperazine rings. The degradation pathway of carbamazepine started with the formation of hydroxyl carbamazepine

and dihydroxy carbamazepine, which turned into acridine as the main transformation product after hydrogen abstraction, decarboxylation, and amine cleavage.

Acknowledgments

The stage of Prof. Hermosilla at the University of Cincinnati was funded by the "*José Castillejo*" mobility program of the Spanish Ministry of Education, Culture, and Sports. Dr. Machala acknowledges the support from the Operational Program "*Research, Development and Education*" of the European Regional Development Fund, and the Czech Ministry of Education, Youth, and Sports for granting project CZ.02.1.01/0.0/0.0/16_019/0000754. This work has also been supported by INHA-60121-1 research grant from INHA University. D. D. Dionysiou also acknowledges support from the University of Cincinnati through a UNESCO co-Chair Professor position on "Water Access and Sustainability" and the Herman Schneider Professorship in the College of Engineering and Applied Sciences. The authors thank Ondřej Malina (Palacký University) for performing magnetization measurements.

References

Alver, A., Karaarslan, M. ,Kilic, A., 2016. The catalytic activity of the iron-coated pumice particles used as heterogeneous catalysts in the oxidation of natural organic matter by H_2O_2. Environ. Technol. 37, 2040-2047.

An, T., Yang, H., Li, G., Song, W., Cooper, W.J., Nie, X., 2010. Kinetics and mechanism of advanced oxidation processes (AOPs) in degradation of ciprofloxacin in water. App. Catal. B Environ. 94, 288-294.

An, J., Zhu, L., Zhang, Y., Tang, H., 2013. Efficient visible light photo-Fenton-like degradation of organic pollutants using in situ surface-modified $BiFeO_3$ as a catalyst. J. Environ. Sci. 25, 1213-1225.

APHA, AWWA, WPCF, 2016. Standard methods for the examination of water and wastewater, 22nd ed. APHA, Washington DC.

Barndõk, H., Hermosilla, D., Cortijo, L., Negro, C., Blanco, A., 2012. Assessing the effect of inorganic anions on TiO_2-photocatalysis and ozone oxidation treatment efficiencies. J. Adv. Oxid. Technol. 15(1), 125-132.

Barndõk, H., Pelaez, M., Han, C., Platten, W.E., Campo, P., Hermosilla, D., Blanco, A., Dionysiou, D.D., 2013. Photocatalytic degradation of contaminants of concern with composite NF-TiO_2 films under visible and solar light. Environ. Sci. Pollut. Res. 20, 3582-3591.

Barndõk, H., Blanco, L., Hermosilla, D., Blanco, A., 2016. Heterogeneous photo-Fenton processes using zero valent iron microspheres for the treatment of wastewaters contaminated with 1,4-dioxane. Chem. Eng. J. 284, 112-121.

Ben Hammouda, S.,Fourcade, F., Assadi, A., Soutrel, I., Adhoum, N., Amrane, A., Monser, L., 2016. Effective heterogeneous electro-Fenton process for the degradation of a malodorous compound, indole, using iron loaded alginate beads as a reusable catalyst. App. Catal. B Environ. 182, 47-58.

Blanco, L., Hermosilla, D., Merayo, N., Blanco, A., 2016. Assessing the use of zero-valent iron microspheres to catalyze Fenton treatment processes. J. Taiwan Inst. Chem. E. 69, 54-60.

Bobu, M., Yediler, A., Siminiceanu, I., Schulte-Hostede, S., 2008. Degradation studies of ciprofloxacin on a pillared iron catalyst. App. Catal. B Environ. 83, 15-23.

Bokare, A.D., Choi, W., 2014. Review of iron-free Fenton-like systems for activating H_2O_2 in advanced oxidation processes. J. Hazard. Mater. 275, 121-135.

Buxton, G.V., Greenstock, C.L., Helman, W.P., Ross, A.B., 1988. Critical review of data constants for reactions of hydrated electrons, hydrogen atoms and hydroxyl radicals in

aqueous solutions. J. Phys. Chem. 17 (2), 513-886.

Council of the European Union, 1998. Council Directive 98/83/EC of 3 November 1998 on the quality of water intended for human consumption. Off. J. Eur. Communities: Legis. L330, 32-54.

Deng, J., Shao, Y., Gao, N., Xia, S., Tan, C., Zhou, S., Hu X., 2013. Degradation of the antiepileptic drug carbamazepine upon different UV-based advanced oxidation processes in water. Chem. Eng. J. 222, 150-158.

Deng, Y., Tang, L., Feng, C., Zeng, G., Chen, Z., Wang, J., Feng, H., Peng, B., Liu, Y., Zhou, Y., 2018. Insight into the dual-channel charge-charrier transfer path for nonmetal plasmonic tungsten oxide based composites with boosted photocatalytic activity under full-spectrum light. App. Catal. B Environ. 235, 225–237.

Desai, I., 2013. Manganese based oxidative technologies for water/wastewater treatment. Texas A&M University, Texas.

Dias, F.F., Oliveira, A.A.S., Arcanjo, A.P., Moura, F.C.C., Pacheco, J.G.A., 2016. Residue-based iron catalyst for the degradation of textile dye via heterogeneous photo-Fenton. App. Catal. B Environ. 186, 136-142.

Dodd, M.C., Shah, A.D., Von Gunten, U., Huang, C.H., 2005. Interactions of fluoroquinolone antibacterial agents with aqueous chlorine: Reaction kinetics, mechanisms, and transformation pathways. Environ. Sci. Technol. 39, 7065-7076.

Du, Y., Ma, W., Liu, P., Zou, B., Ma, J., 2016. Magnetic $CoFe_2O_4$ nanoparticles supported on titanate nanotubes ($CoFe_2O_4$/TNTs) as a novel heterogeneous catalyst for peroxymonosulfate activation and degradation of organic pollutants. J. Hazard. Mater. 308, 58-66.

Fiorentino, A., Esteban, B., Garrido-Cardenas, J.A., Kowalska, K., Rizzo, L., Aguera, A., Sánchez Pérez, J.A., 2019. Effect of solar photo-Fenton process in raceway pond reactors

at neutral pH on antibiotic resistance determinants in secondary treated urban wastewater. J. Hazard. Mater. 378, 120737.

Flanagan, J., Kortegaard, K., Pinder, D.N., Rades, T., Singh, H., 2006. Solubilisation of soybean oil in microemulsions using various surfactants. Food Hydrocolloids 20, 253-260.

Giri, A.S., Golder, A.K., 2014. Ciprofloxacin degradation from aqueous solution by Fenton oxidation: reaction kinetics and degradation mechanisms. RSC Adv. 4, 6738-6745.

Giri, A.S., Golder, A.K., 2019. Ciprofloxacin degradation in photo-Fenton and photo-catalytic processes: Degradation mechanisms and iron chelation. J. Environ. Sci. 80, 82-92.

Goldman, A., 2006. Modern ferrite techology. Springer, Pittsburg.

Guan, Y.-H., Ma, J., Ren, Y.-M., Liu, Y.-L., Xiao, J.-Y., Lin, L.-Q., Zhang, C., 2013. Efficient degradation of atrazine by magnetic porous copper ferrite catalyzed peroxymonosulfate oxidation via the formation of hydroxyl and sulfate radicals. Water Res. 47, 5431-5438.

Hao, C., Clement, R., Yang, P., 2007. Liquid chromatography-tandem mass spectrometry of bioactive pharmaceutical compounds in the aquatic environment - a decade's activities. Anal. Bioanal. Chem. 387, 1247-1257.

Hashim, M., Shirsath, S.E., Meena, S.S., Mane, M.L., Kumar, S., Bhatt, P., Kumar, R., Prasad, N.K., Alla, S.K., Shah, J., Kotnala, R.K., Mohammed, K.A., Senturk, E., Alimuddin, 2015. Manganese ferrite prepared using reverse micelle process: Structural and magnetic properties characterization. J. Alloys Compd. 642, 70-77.

Hermosilla, D., Cortijo, M., Huang, C.P., 2009a. Optimizing the treatment of landfill leachate by conventional Fenton and photo-Fenton processes. Sci. Total Environ. 407, 3473-3481.

Hermosilla, D., Cortijo, M., Huang, C.P., 2009b. The role of iron on the degradation and mineralization of organic compounds using conventional Fenton and photo-Fenton

processes. Chem. Eng. J. 155, 637-646.

Hermosilla, D., Merayo, N., Ordóñez, R., Blanco, A., 2012. Optimization of conventional Fenton and ultraviolet-assisted oxidation processes for the treatment of reverse osmosis retentate from a paper mill. Waste Manag. 32, 1236-1243.

Hermosilla, D., Merayo, N., Gasco, A., Blanco, A., 2015. The application of advanced oxidation technologies to the treatment of effluents from the pulp and paper industry: a review. Environ. Sci. Pollut. Res. 22, 168-191.

Ikehata, K., Gamal El-Din, M., Snyder, S.A., 2008. Ozonation and advanced oxidation treatment of emerging organic pollutants in water and wastewater. Ozone: Sci. Eng. 30, 21-26.

Jiang, J., Zou, J., Anjum, M.N., Yan, J., Huang, L., Zhang, Y., Chen, J., 2011. Synthesis and characterization of wafer-like $BiFeO_3$ with efficient catalytic activity. Solid State Sci. 13, 1779-1785.

Jiang, L., Yuan, X., Zeng, G., Chen, X., Wu, Z., Liang, J., Zhang, J., Wang, H., Wang, H., 2017. Phosphorus- and sulfur-codoped g-C_3N_4: facile preparation, mechanism insight, and application as efficient photocatalyst for tetracycline and methyl orange degradation under visible light irradiation. ACS Sustain. Chem. Eng. 5(7), 5831-5841.

Jin, Y., Wang, X., Sun, S.-P., Dong, W., Wu, Z., Bian, G., Wu, W.D., Chen, X.D., 2019. Hydroxyl and sulfate radicals formation in UVA/FeIII-NTA/$S_2O_8^{2-}$ system: Mechanism and effectiveness in carbamazepine degradation at initial neutral pH, Chem. Eng. J. 368, 541-552.

Kavitha, V., Palanivelu, K., 2004. The role of ferrous ion in Fenton and photo-Fenton processes for the degradation of phenol. Chemosphere 55, 1235-1243.

Kim, S.M. Geissen, S.U. Vogelpohl, A., 1997. Landfill leachate treatment by a photoassisted Fenton reaction. Water Sci. Technol. 35, 239-248.

Kim, D.-H., Nikles, D.E., Brazel, C.S., 2010. Synthesis and characterization of multi-functional chitosan-$MnFe_2O_4$ nanoparticles for magnetic hyperthermia and drug delivery. Mater. 3, 4051-4065.

Kishimoto, N., Kitamura, T., Kato, M., Otsu, H., 2013. Reusability of iron sludge as an iron source for the electrochemical Fenton-type process using Fe^{2+}/HOCl system. Water Res. 47, 1919-1927.

Klamerth, N., Malato, S., Agüera, A., Fernández-Alba, A., Mailhot, G., 2012. Treatment of municipal wastewater treatment plant effluents with modified photo-Fenton as a tertiary treatment for the degradation of micro pollutants and disinfection. Environ. Sci. Technol. 46, 2885-2892.

Lima, M.J., Leblebici, M.E., Dias, M.M., Lopes, J.C.B., Silva, C.G., Silva, A.M.T., Faria, J.L., 2014. Continuous flow photo-Fenton treatment of ciprofloxacin in aqueous solutions using homogeneous and magnetically recoverable catalysts. Environ. Sci. Pollut. Res. 21, 11116-11125.

Lima Perini, J.A. de, Perez-Moya, M., Pupo Nogueira, R.F., 2013. Photo-Fenton degradation kinetics of low ciprofloxacin concentration using different iron sources and pH. J Photochem. Photobiol. A Chem. 259, 53-58.

Liu, S.-Q., Feng, L.-R., Xu, N., Chen, Z.-G., Wang, X.-M., 2012. Magnetic nickel ferrite as a heterogeneous photo-Fenton catalyst for the degradation of rhodamine B in the presence of oxalic acid. Chem. Eng. J. 203, 432-439.

Lubej, M., Kalcikova, G., Plazl, I., Gotvajn, A.Z., 2016. Feasibility of carbon nanofiber catalyst support for the heterogeneous Fenton process. J. Environ. Eng. 142(12), 3968-3978.

Mahmoodi, N.M., 2013. Zinc ferrite nanoparticle as a magnetic catalyst: Synthesis and dye degradation. Mater. Res. Bull. 48, 4255-4260.

Masala, O., Seshadri, R., 2005. Magnetic properties of capped, soluble $MnFe_2O_4$ nano-particles. Chem. Phys. Lett. 402, 160-164.

Mendonca, C.R.B., Silva, Y.P., Bockel, W.J., Simo-Alfonso, E.F., Ramis-Ramos, G., Piatnicki, C.M.S., Bica, C.I.D., 2009. Role of the co-surfactant nature in soybean w/o microemulsions. J. Colloid Interface Sci. 337, 579-585.

Merayo, N., Hermosilla, D., Blanco, L., Cortijo, L., Blanco, A., 2013a. Assessing the application of advanced oxidation processes, and their combination with biological treatment, to effluents from pulp and paper industry. J. Hazard. Mater. 262, 420-427.

Merayo, N., Hermosilla, D., Negro, C., Blanco, A., 2013b. On-line FTIR as a novel tool to monitor Fenton process behavior. Chem. Eng. J. 232, 519-526.

Mohapatra, D.P., Brar, S.K., Tyagi, R.D., Picard, P., Surampalli, R.Y., 2012. Carbamazepine in municipal wastewater and wastewater sludge: Ultrafast quantification by laser diode thermal desorption-atmospheric pressure chemical ionization coupled with tandem mass spectrometry. Talanta 99, 247-255.

Mohapatra, D.P., Brar, S.K., Tyagi, R.D., Picard, P., Surampalli, R.Y., 2014. Analysis and advanced oxidation treatment of a persistent pharmaceutical compound in wastewater and wastewater sludge-carbamazepine. Sci. Total Environ. 470, 58-75.

Moreira, F.C., Boaventura, R.A.R., Brillas, E., Vilar, V.J.P., 2017. Electrochemical advanced oxidation processes: A review on their application to synthetic and real wastewaters. App. Catal. B Environ. 202, 217-261.

Nawaz, M., Miran, W., Jang, J., Lee, D.S., 2017. One-step hydrothermal synthesis of porous 3D reduced graphene oxide/TiO_2 aerogel for carbamazepine photodegradation in aqueous solution. App. Catal. B Environ. 203, 85-95.

Nowara, A., Burhenne, J., Spiteller, M., 1997. Binding of fluoroquinolone carboxylic acid derivatives to clay minerals. J. Agric. Food Chem. 45, 1459-1463.

OECD, 2015. Pharmaceutical sector, in: Health at a Glance 2015: OECD Indicators. OECD Publishing, Paris, pp. 177-188.

Rivas, F.J., Beltran, F.J., Gimeno, O., Alvarez, P., 2003. Treatment of brines by combined Fenton's reagent-aerobic biodegradation II. Process modelling. J. Hazard. Mater. 96, 259-276.

Rodriguez, R., Espada, J.J., Pariente, M.I., Melero, J.A., Martínez, F., Molina, R., 2016. Comparative life cycle assessment (LCA) study of heterogeneous and homogenous Fenton processes for the treatment of pharmaceutical wastewater. J. Cleaner Prod. 124, 21-29.

Sharma, R., Singhal, S., 2015. Photodegradation of textile dye using magnetically recyclable heterogeneous spinel ferrites. J. Chem. Technol. Biotechnol. 90, 955-962.

Takacsnovak, K., Jozan, M. ,Hermecz, I., Szasz, G., 1992. Lipophilicity of antibacterial fluoroquinolones. Int. J. Pharm. 79, 89-96.

Torniainen, K., Tammilehto, S., Ulvi, V., 1996. The effect of pH, buffer type and drug concentration on the photodegradation of ciprofloxacin. Int. J. Pharm. 132, 53-61.

Wan, J., Deng, H., Shi, J., Zhou, L., Su, T., 2014. Synthesized magnetic manganese ferrite nanoparticles on activated carbon for sulfamethoxazole removal. Clean: Soil, Air, Water 42, 1199-1207.

Wang, H., Wu, Y., Feng, M., Tu, W., Xiao, T., Xiong, T., Ang, H., Yuan, X., Chew, J.W., 2018a. Visible-light-driven removal of tetracycline antibiotics and reclamation of hydrogen energy from natural water matrices and wastewater by polymeric carbon nitride foam. Water Res. 144, 215-225.

Wang, H., Wu, Y., Xiao, T., Yuan, X., Zeng, G., Tu, W., Wu, S., Lee, H.Y., Tan, Y.Z., Chew, J.W., 2018b. Formation of quasi-core-shell In_2S_3/anatase TiO_2@metallic $Ti_3C_2T_x$ hybrids with favorable charge transfer channels for excellent visible-light photocatalytic performance. App. Catal. B Environ. 233, 213-225.

Wang, H., Sun, Y., Wu, Y., Tu, W., Wu, S., Yuan, X., Zeng, G., Xu, Z.J., Li, S., Chew, J.W., 2019. Electrical promotion of spatially photoinduced charge separation via interfacial-built-in quasi-alloying effect in hierarchical $Zn_2In_2S_5/Ti_3C_2(O,OH)_x$ hybrids toward efficient photocatalytic hydrogen evolution and environmental remediation. App. Catal. B Environ. 245, 290-301.

Wang, M., Fang, G., Liu, P., Zhou, D., Ma, C., Zhang, D., Zhan, J., 2016. Fe_3O_4@beta-CD nanocomposite as heterogeneous Fenton-like catalyst for enhanced degradation of 4-chlorophenol (4-CP). App. Catal. B Environ. 188, 113-122.

Wang, W.L., Wu, Q.Y., Huang, N., Wang, T., Hu, H.-Y., 2016. Synergistic effect between UV and chlorine (UV/chlorine) on the degradation of carbamazepine: Influence factors and radical species. Water Res. 98, 190-198.

Wang, X., Lin, Y., Ding, X., Jiang, J., 2011. Enhanced visible-light-response photocatalytic activity of bismuth ferrite nanoparticles. J. Alloys Compd. 509, 6585-6588.

Watkinson, A.J., Murby, E.J., Costanzo, S.D.. 2007. Removal of antibiotics in conventional and advanced wastewater treatment: Implications for environmental discharge and wastewater recycling. Water Res. 41, 4164-4176.

Wu, Y., Wang, H., Tu, W., Liu, Y., Tan, Y.Z., Yuan, X., Chew, J.W., 2018. Quasi-polymeric construction of stable perovskite-type $LaFeO_3/g\text{-}C_3N_4$ heterostructured photocatalyst for improved Z-scheme photocatalytic activity via solid p-n heterojunction interfacial effect. J. Hazard. Mater. 347, 412-422.

Yang, B., Kookana, R.S., Williams, M., Du, J., Doan, H., Kumar, A., 2016. Removal of carbamazepine in aqueous solutions through solar photolysis of free available chlorine. Water Res. 100, 413-420.

Yang, X., Zhang, Y., Xu, G., Wei, X., Ren, Z., Shen, G., Han, G., 2013. Phase and morphology evolution of bismuth ferrites via hydrothermal reaction route. Mater. Res.

Bull. 48, 1694-1699.

Yuan, X., Jiang, L., Chen, X., Leng, L., Wang, H., Wu, Z., Xiong, T., Liang, J., Zeng, G., 2017. Highly efficient visible-light-induced photoactivity of Z-scheme Ag_2CO_3/Ag/WO_3 photocatalysts for organic pollutant degradation. Environ. Sci.: Nano 4(11), 2175-2185.

Zhang, H.C., Huang, C.H., 2005. Oxidative transformation of fluoroquinolone antibacterial agents and structurally related amines by manganese oxide. Environ. Sci. Technol. 39, 4474-4483.

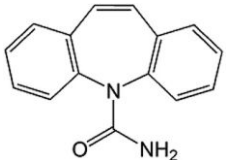
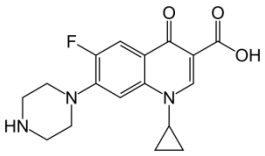
Zhang, K., Wang, L., Sheng, X., Ma, M., Jung, M.S., Kim, W., Lee, H., Park, J.H., 2016. Tunable bandgap energy and promotion of H_2O_2 oxidation for overall water splitting from carbon nitride nanowire bundles. Adv. Energy Mater 6, 1502352.

Zhang, S., Gao, H., Liu, X., Huang, Y., Xu, X., Alharbi, N.S., Hayat, T., Li, J., 2016. Hybrid 0D-2D nanoheterostructures: in situ growth of amorphous silver silicates dots on g-C_3N_4 nanosheets for full-spectrum photocatalysis. ACS Appl. Mater. Interfaces 8(51), 35138-35149.

Zhang, Y., Geissen, S.-U., Gal, C., 2008. Carbamazepine and diclofenac: Removal in wastewater treatment plants and occurrence in water bodies. Chemosphere 73, 1151-1161.

Zhu, L., Santiago-Schübel, B., Xiao, H., Hollert, H., Kueppers, S., 2016. Electrochemical oxidation of fluoroquinolone antibiotics: Mechanism, residual antibacterial activity and toxicity change. Water Res. 102, 52-62.

Table 1. Physicochemical properties of carbamazepine and ciprofloxacin.

Name	Chemical formula	Chemical structure	Molecular weight (g mol^{-1})	Water solubility (mg L^{-1}, 20 °C)	Log Kow	pKa
Carbamazepine	$C_{15}H_{12}N_2O$		236.27	17.7	2.45*	13.9*
Ciprofloxacin	$C_{17}H_{18}FN_3O_3$		331.35	30 **	0.28***	6.09****

References: www.chemicalbook.com, www.SigmaAldrich.com, www.alfa.com.

* (Deng et al., 2013)
** (Nowara et al., 1997)
*** (Takacsnovak et al., 1992)
**** (Torniainen et al., 1996)

Table 2. Characteristics of the biologically-treated domestic effluent from a pilot WWTP (University of Cincinnati, USA).

Parameter	Value
pH	8
Alkalinity, mg $CaCO_3$ L^{-1}	135
Conductivity, mS cm^{-1}	1.14
Turbidity, mNTU	136.6
COD, mg L^{-1}	25
TOC, mg L^{-1}	5
N-NH_4^+, mg L^{-1}	2.9
N-NO_3^-, mg L^{-1}	14.6

Table 3. Surface area of ferrite nanomaterials synthesized by different procedures.

Synthesis method	**Surface area, $m^2 g^{-1}$**
Sol-gel $MnFe_2O_4$	43.82
Sol-gel Fe_3O_4	15.12
Combustion $MnFe_2O_4$	76.96
Combustion $Mn_{0.5}Fe_{2.5}O_4$	75.00
Combustion without cellulose $MnFe_2O_4$	177.75
Combustion Fe_3O_4	25.05
Microemulsion $MnFe_2O_4$	5.27
Microemulsion Fe_3O_4	6.05

Table 4. SEM Characterization of the synthesized ferrites.

Synthesis process	Element	Weight %	Atomic %	Compound %	Formula
Combustion	Mn K	50.61	32.82	65.35	MnO
	Fe K	26.93	17.18	34.65	FeO
	O	22.45	50.00		
Sol-gel	Mn K	31.39	20.42	40.53	MnO
	Fe K	46.23	29.58	59.47	FeO
	O	22.38	50.00		
Microemulsion	Mn K	9.39	6.13	12.13	MnO
	Fe K	68.30	43.87	87.87	FeO
	O	22.30	50.00		

Table 5. Magnetization at room temperature and relative contents of iron bearing phases measured by Mössbauer spectroscopy (at % of Fe) of synthesized ferrites.

.

Sample	Magnetization [emu g^{-1}]	Fe component	Relative content [at % Fe]
Sol-gel $MnFe_2O_4$	41.0	$MnFe_2O_4$	92
		α-Fe_2O_3	8
Microemulsion $MnFe_2O_4$	3.7	$MnFe_2O_4$	4 (SP)
		α-Fe_2O_3	96
Combustion $MnFe_2O_4$	22.8	$MnFe_2O_4$	81 (35 SP)
		α-Fe_2O_3	19
Sol-gel Fe_3O_4	1.7	α-Fe_2O_3	100
Microemulsion Fe_3O_4	3.5	α-Fe_2O_3	98
		Fe_2O_3 SP	2
Combustion Fe_3O_4	5.7	α-Fe_2O_3	79
		Fe_2O_3 SP	21

Note: SP = superparamagnetic phase

Figure captions

Figure 1. SEM images of Fe_3O_4 particles synthesized by combustion (a), reverse microemulsion (b), and sol-gel (c) processes; and $MnFe_2O_4$ nanomaterials synthesized by combustion (d), reverse microemulsion (e), and sol-gel (f) processes.

Figure 2. TEM and HR-TEM images of $MnFe_2O_4$ nanomaterials synthesized by combustion (a and d), reverse microemulsion (b and e), and sol-gel processes (c and f).

Figure 3. XRD patterns of synthesized $MnFe_2O_4$ samples and control ferrite.

Figure 4. XPS spectra of $MnFe_2O_4$ nanomaterials synthesized by combustion (a) and sol-gel (b) processes.

Figure 5. Hysteresis loop, measured at T = 300 K, where M_{max+} (9T) is maximum magnetization at 9T, M_{max-} (–9T) is maximum magnetization at –9T, H_{C+} is positive coercivity, H_{C-} is negative coercivity, M_{R+} is positive remnant magnetization, and M_{R-} is negative remnant magnetization [a) sol-gel $MnFe_2O_4$, b) combustion $MnFe_2O_4$, c) reverse microemulsion $MnFe_2O_4$ and d) sol-gel Fe_3O_4].

Figure 6. Degradation of ciprofloxacin by the solar photo-Fenton treatment using each synthesized catalyst ($[H_2O_2]$/COD = 4.250 and $[H_2O_2]$/[Fe, Mn] = 5).

Figure 7. Degradation of ciprofloxacin and carbamazepine present in domestic wastewater by the solar photo-Fenton treatment using the sol-gel synthesized Mn-ferrite as catalyst ($[H_2O_2]$/COD = 4.250 and $[H_2O_2]$/[Fe, Mn] = 5).

Figure 8. Degradation of (a) carbamazepine and (b) ciprofloxacin by the solar photo-Fenton treatment using the sol-gel synthesized Mn-ferrite as catalyst ($[H_2O_2]$/COD = 4.250 and $[H_2O_2]$/[Fe, Mn] = 5).

Figure 9. Reuse cycles of the sol-gel synthesized Mn-ferrite applied to the photo-Fenton treatment of ciprofloxacin ($[H_2O_2]$/COD = 4.250 and $[H_2O_2]$/[Fe, Mn] = 5).

Figure 10. Possible degradation routes of ciprofloxacin.

Figure 11. Possible degradation routes of carbamazepine.

Figure SI1. Room temperature Mössbauer spectra of sol-gel $MnFe_2O_4$ (a), microemulsion $MnFe_2O_4$ (b), combustion $MnFe_2O_4$ (c), sol-gel Fe_3O_4 (d), microemulsion Fe_3O_4 (e), and combustion Fe_3O_4 (f). sp: superparamagnetic phase, rc: relaxation component.

FIGURE 1

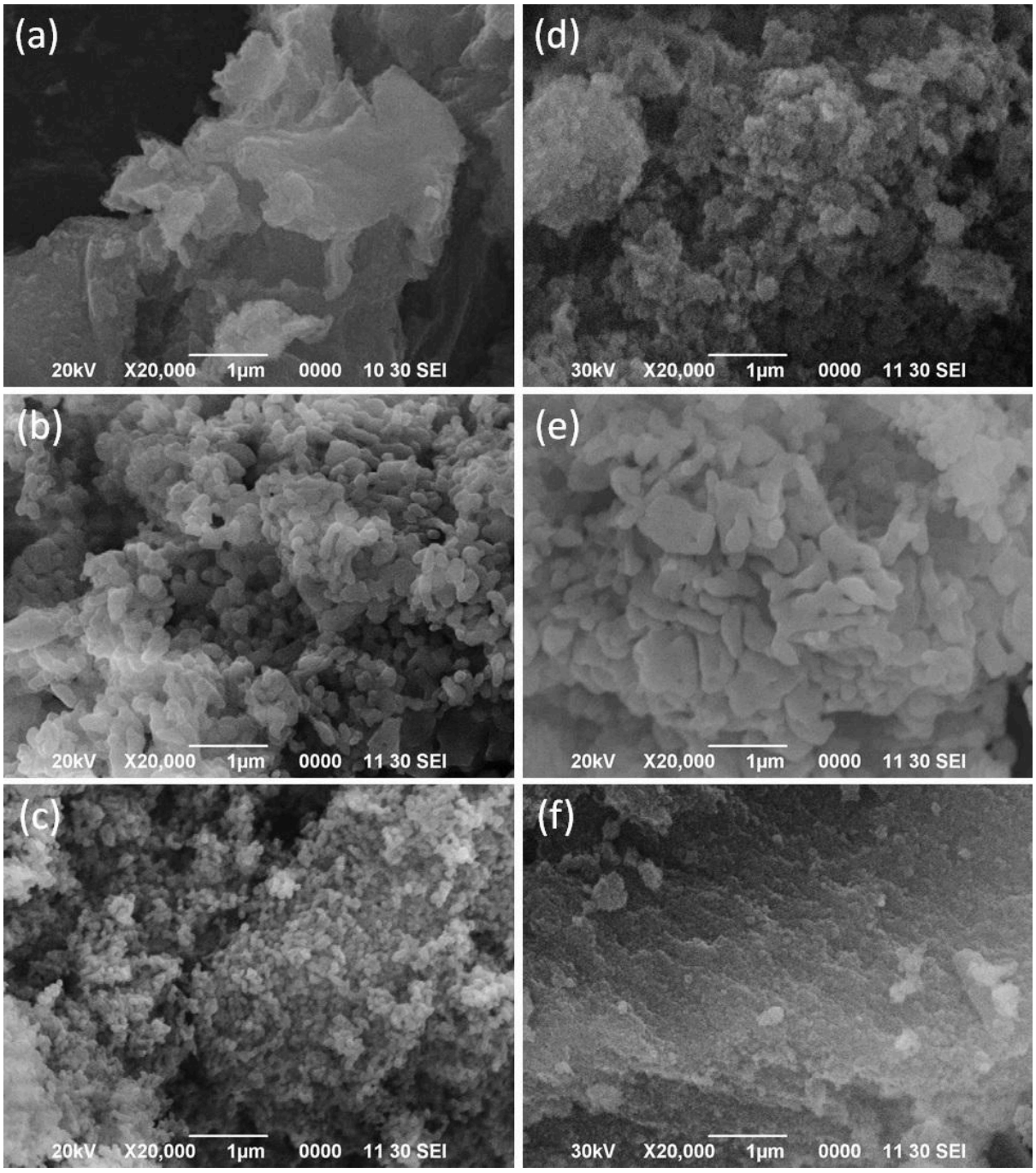

(a)
20kV X20,000 1μm 0000 10 30 SEI
(d)
30kV X20,000 1μm 0000 11 30 SEI
(b)
20kV X20,000 1μm 0000 11 30 SEI
(e)
20kV X20,000 1μm 0000 11 30 SEI
(c)
20kV X20,000 1μm 0000 11 30 SEI
(f)
30kV X20,000 1μm 0000 11 30 SEI

FIGURE 2

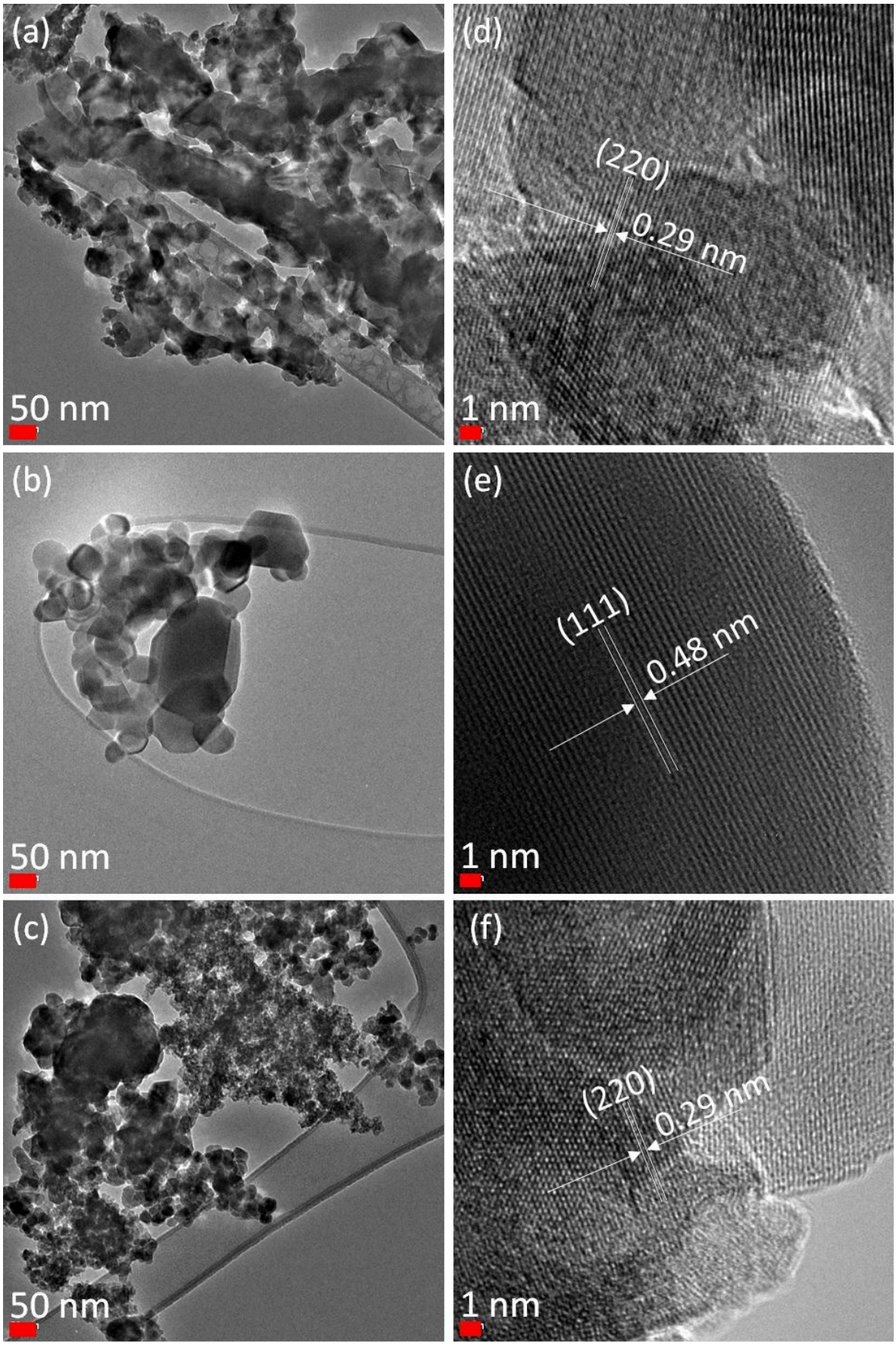

(a)
50 nm
(d)
(220)
0.29 nm
1 nm
(b)
50 nm
(e)
(111)
0.48 nm
1 nm
(c)
50 nm
(f)
(220)
0.29 nm
1 nm

FIGURE 3

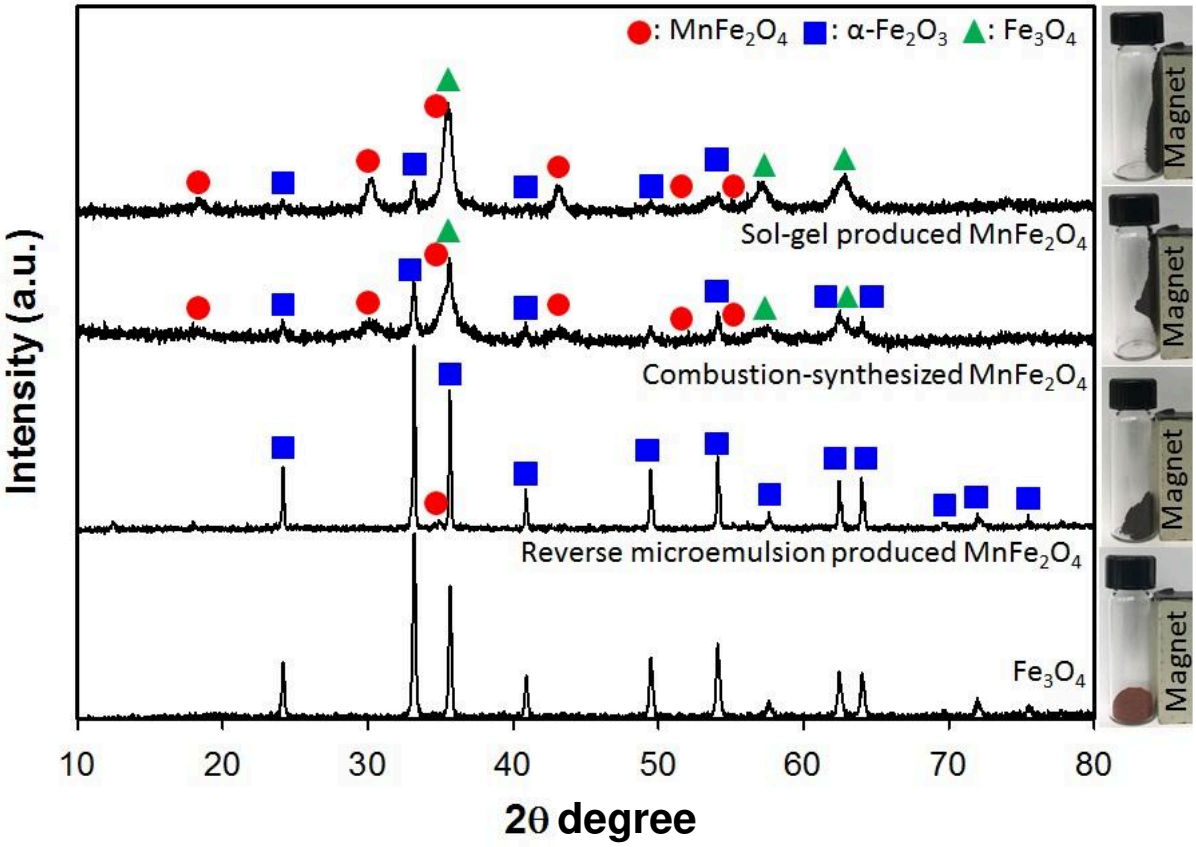

●: MnFe2O4 ■: α-Fe2O3 ▲: Fe3O4
Sol-gel produced MnFe2O4
Combustion-synthesized MnFe2O4
Reverse microemulsion produced MnFe2O4
Fe3O4
Magnet
Magnet
Magnet
Magnet
Intensity (a.u.)
10
20
30
40
50
60
70
80
2θ degree

FIGURE 4

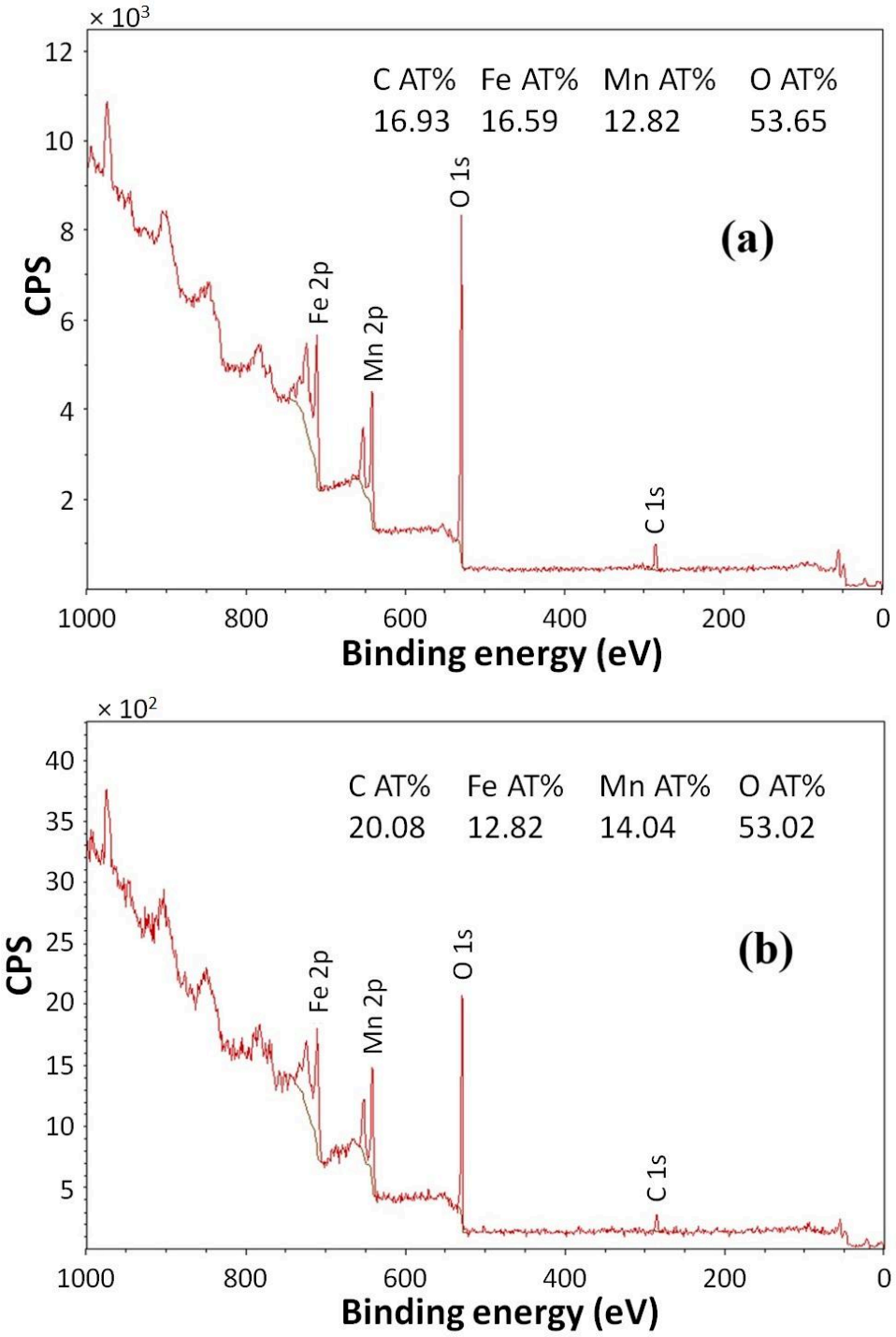

× 10³
C AT% Fe AT% Mn AT% O AT%
16.93 16.59 12.82 53.65
O 1s
(a)
Fe 2p
Mn 2p
C 1s
CPS
Binding energy (eV)
× 10²
C AT% Fe AT% Mn AT% O AT%
20.08 12.82 14.04 53.02
(b)
Fe 2p
Mn 2p
O 1s
C 1s
CPS
Binding energy (eV)

FIGURE 5

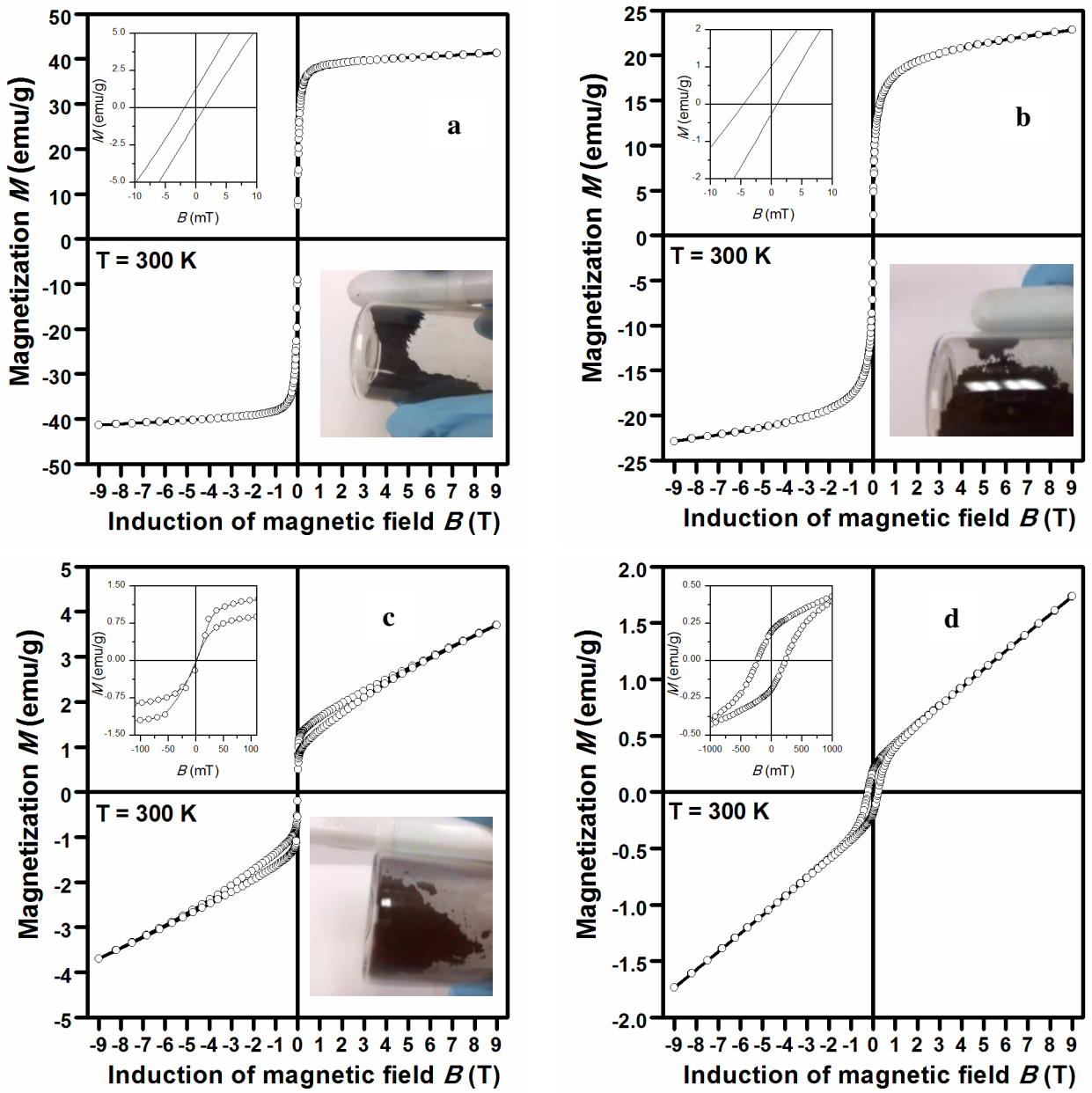

a
T = 300 K
Magnetization M (emu/g)
Induction of magnetic field B (T)
M (emu/g)
B (mT)
b
T = 300 K
Magnetization M (emu/g)
Induction of magnetic field B (T)
M (emu/g)
B (mT)
c
T = 300 K
Magnetization M (emu/g)
Induction of magnetic field B (T)
M (emu/g)
B (mT)
d
T = 300 K
Magnetization M (emu/g)
Induction of magnetic field B (T)
M (emu/g)
B (mT)

FIGURE 6

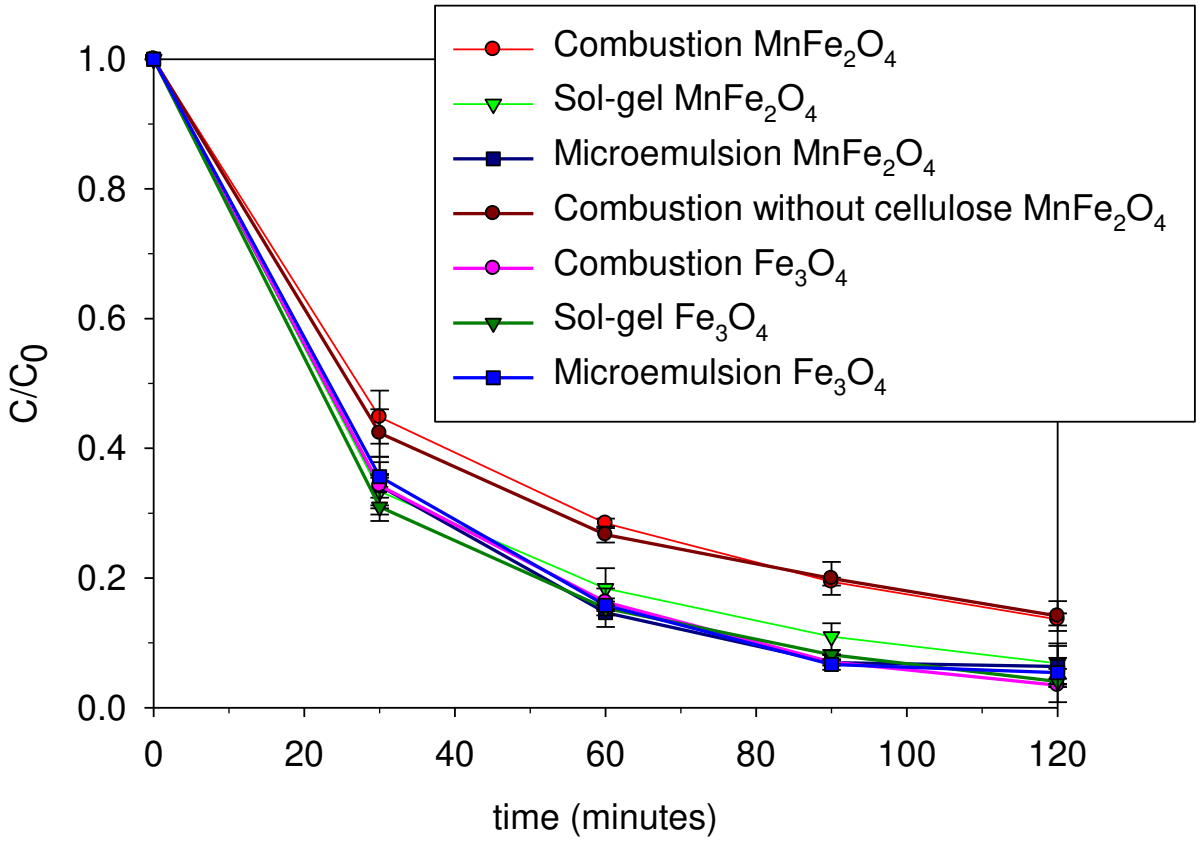

Combustion $MnFe_2O_4$
Sol-gel $MnFe_2O_4$
Microemulsion $MnFe_2O_4$
Combustion without cellulose $MnFe_2O_4$
Combustion Fe_3O_4
Sol-gel Fe_3O_4
Microemulsion Fe_3O_4
C/C0
1.0
0.8
0.6
0.4
0.2
0.0
0
20
40
60
80
100
120
time (minutes)

FIGURE 7

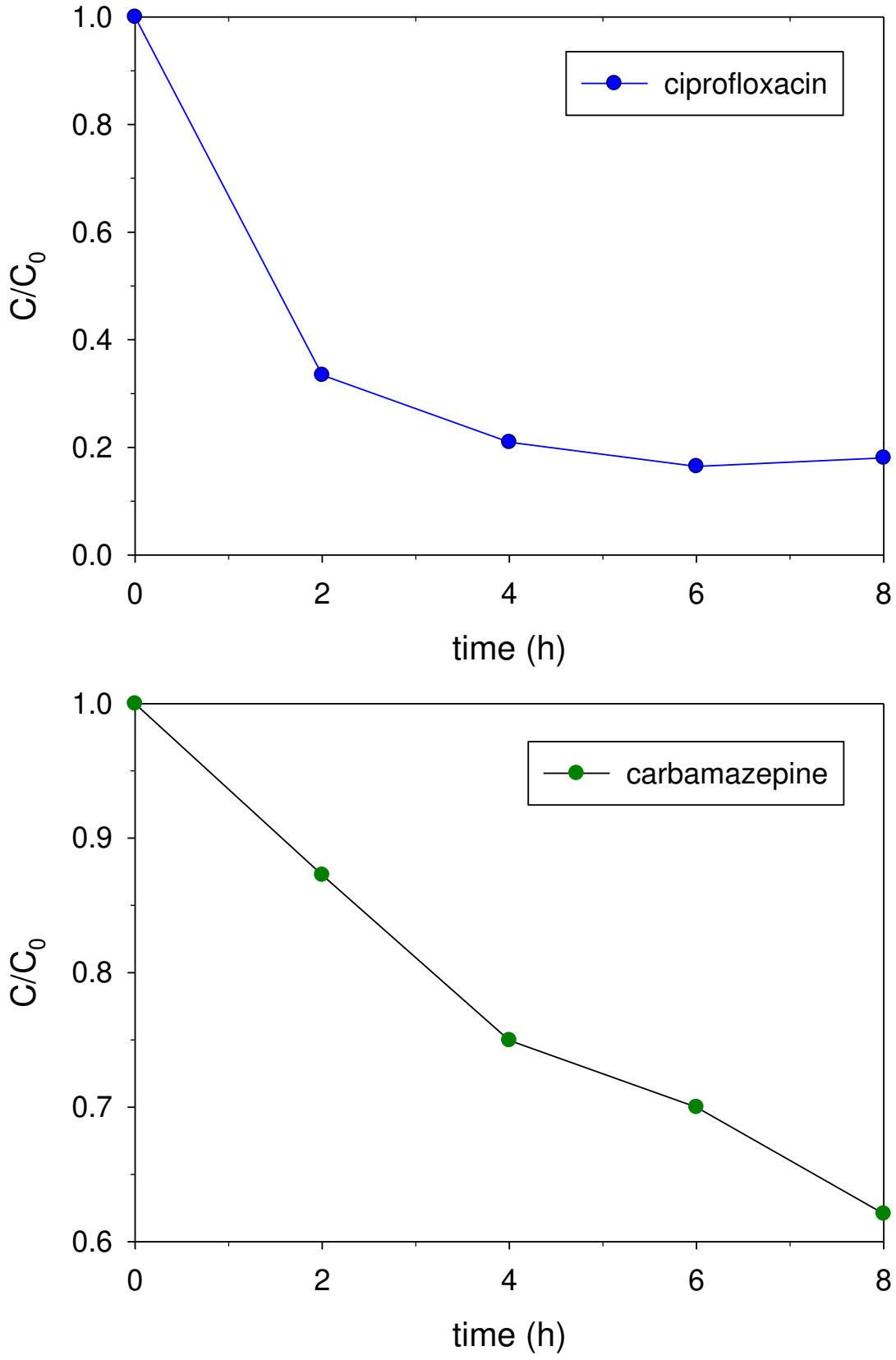

1.0
0.8
0.6
0.4
0.2
0.0
C/C0
ciprofloxacin
0
2
4
6
8
time (h)
1.0
0.9
0.8
0.7
0.6
C/C0
carbamazepine
0
2
4
6
8
time (h)

FIGURE 8

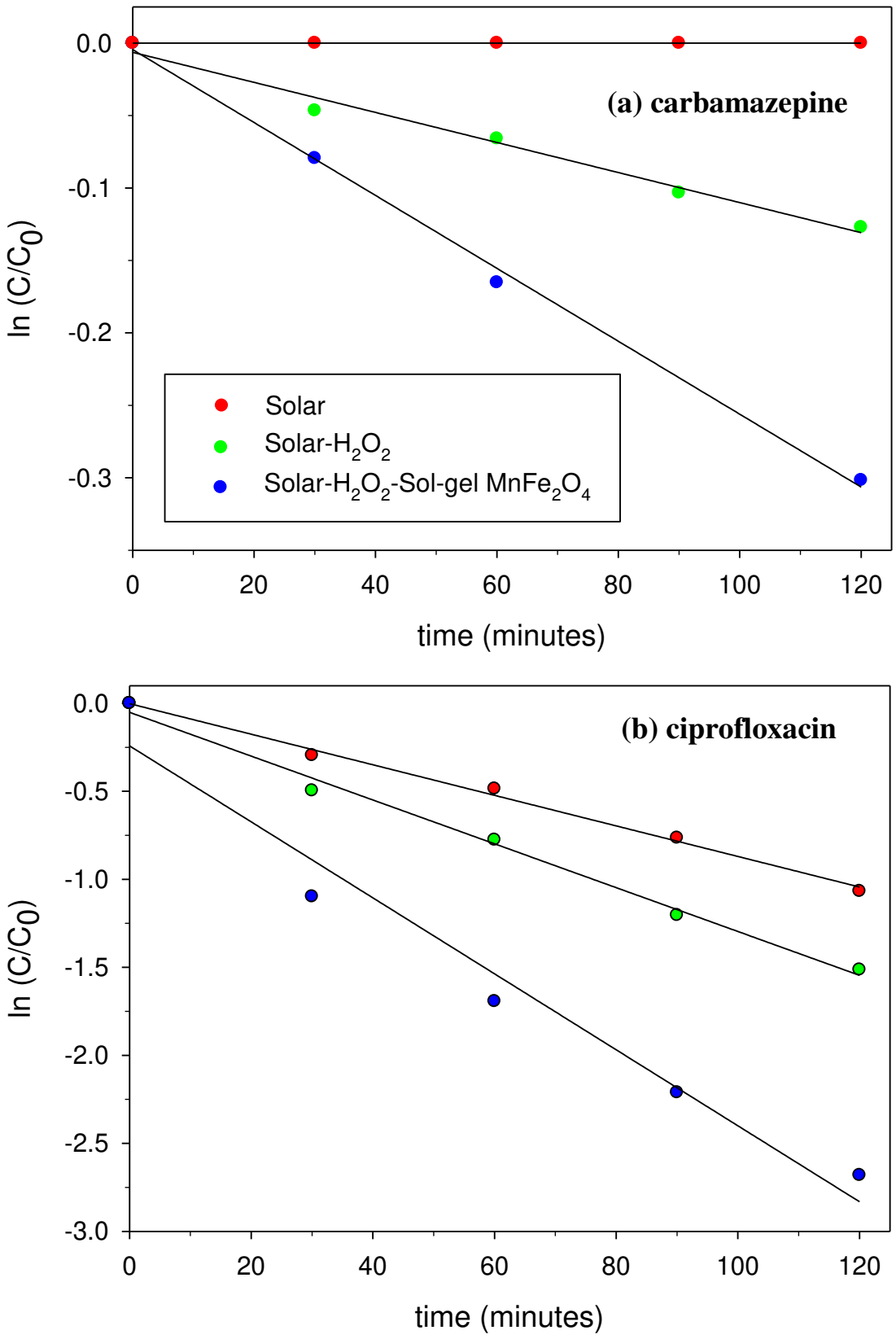

(a) carbamazepine
Solar
Solar-H2O2
Solar-H2O2-Sol-gel MnFe2O4
ln (C/C0)
time (minutes)
0.0
-0.1
-0.2
-0.3
0
20
40
60
80
100
120
(b) ciprofloxacin
ln (C/C0)
time (minutes)
0.0
-0.5
-1.0
-1.5
-2.0
-2.5
-3.0

FIGURE 9

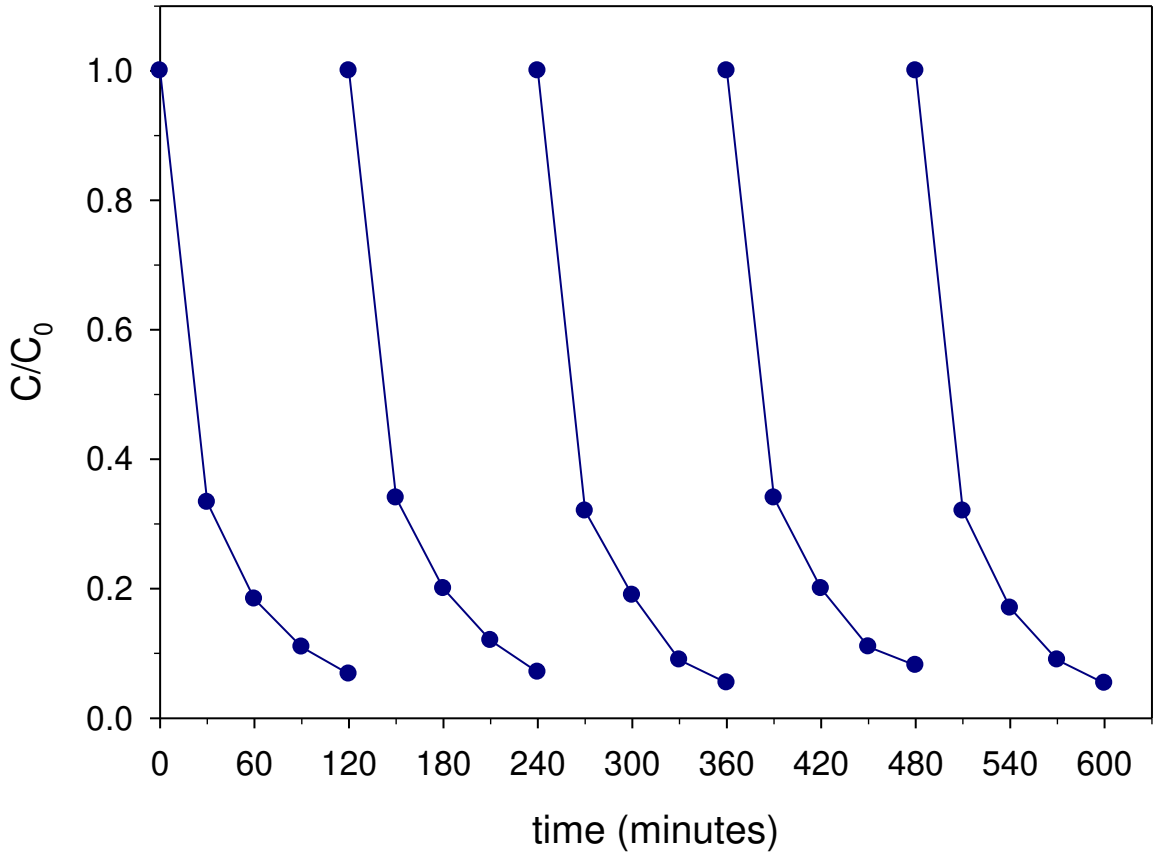

1.0
0.8
0.6
0.4
0.2
0.0
C/C0
0
60
120
180
240
300
360
420
480
540
600
time (minutes)

FIGURE 10

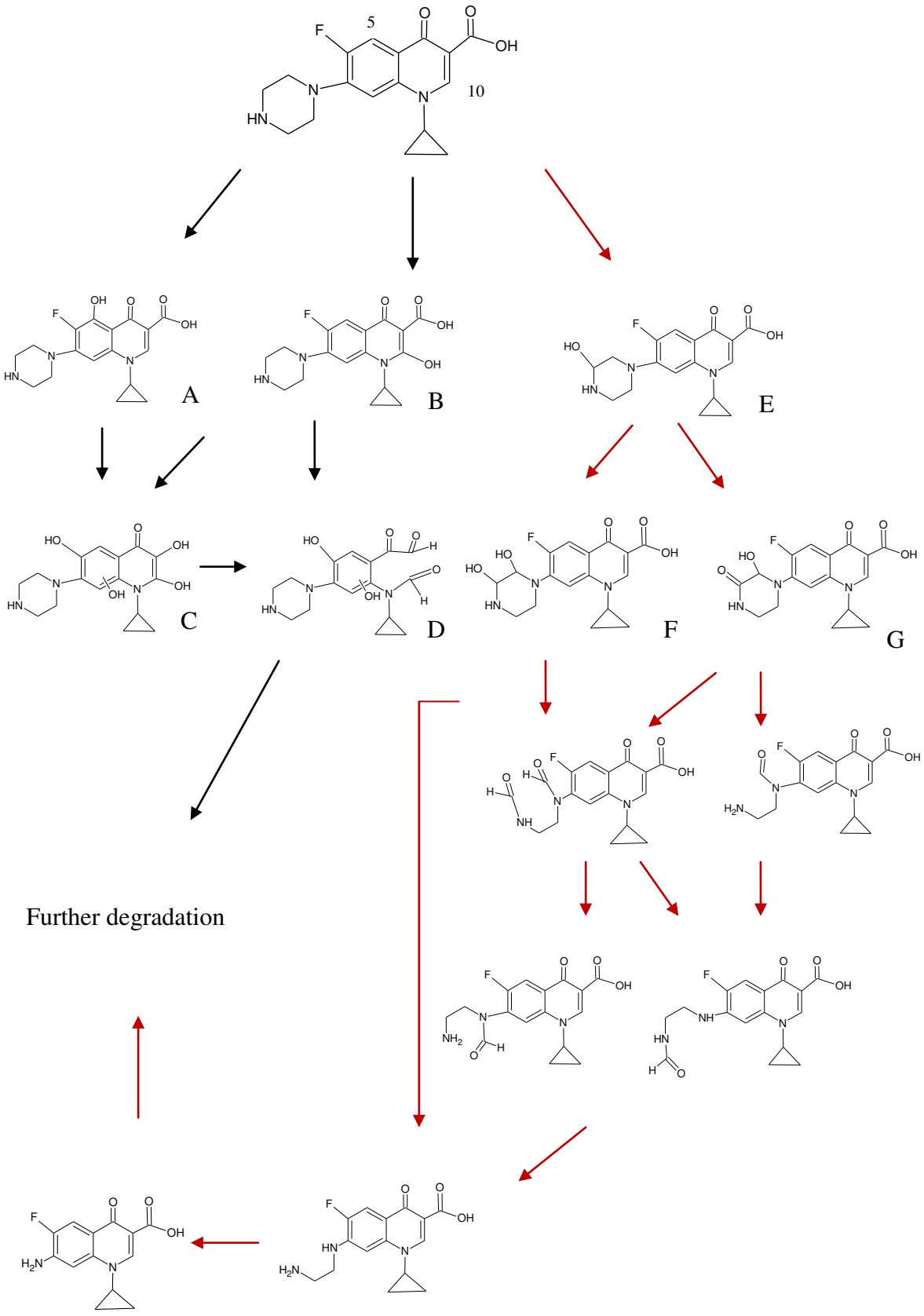


FIGURE 11

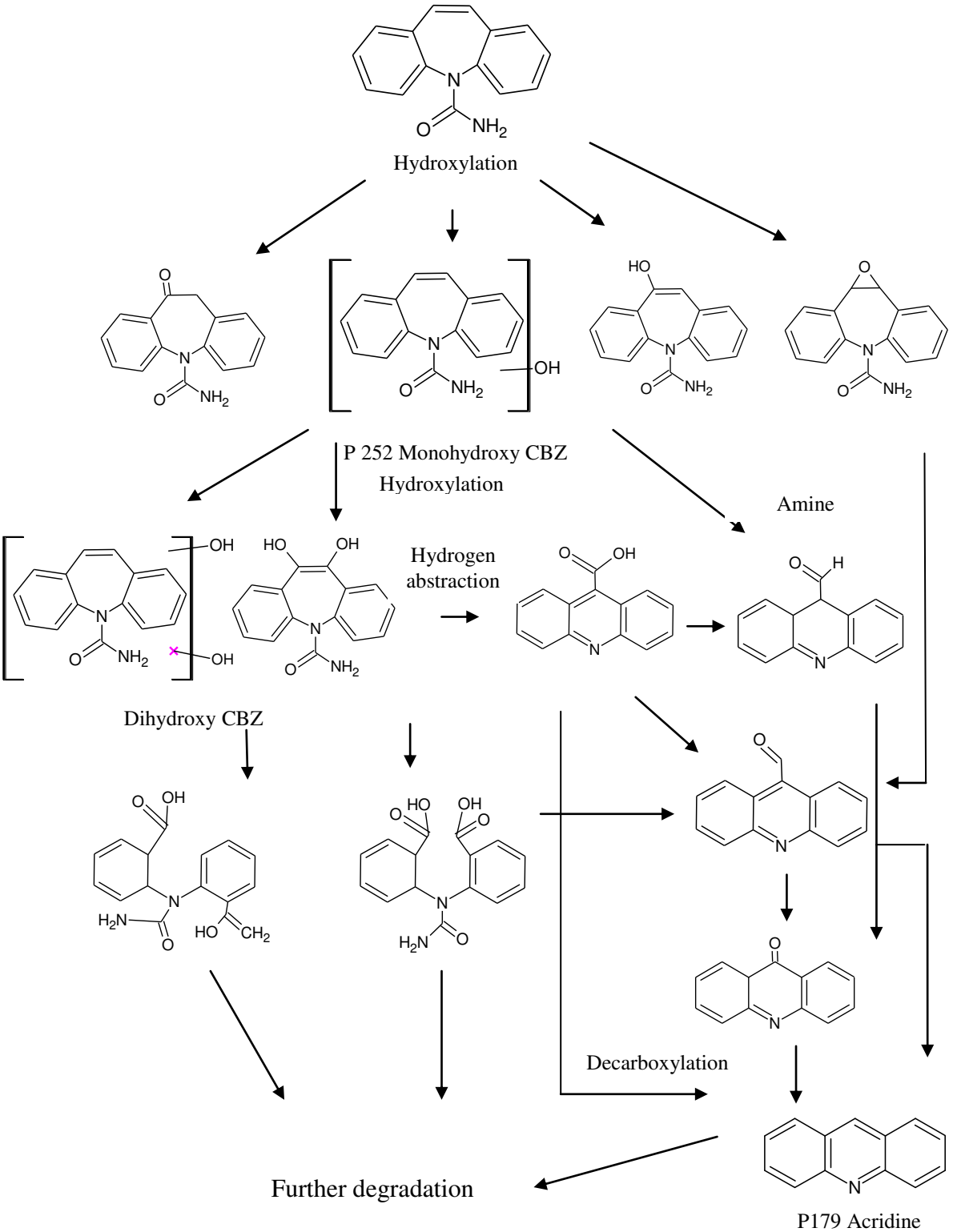
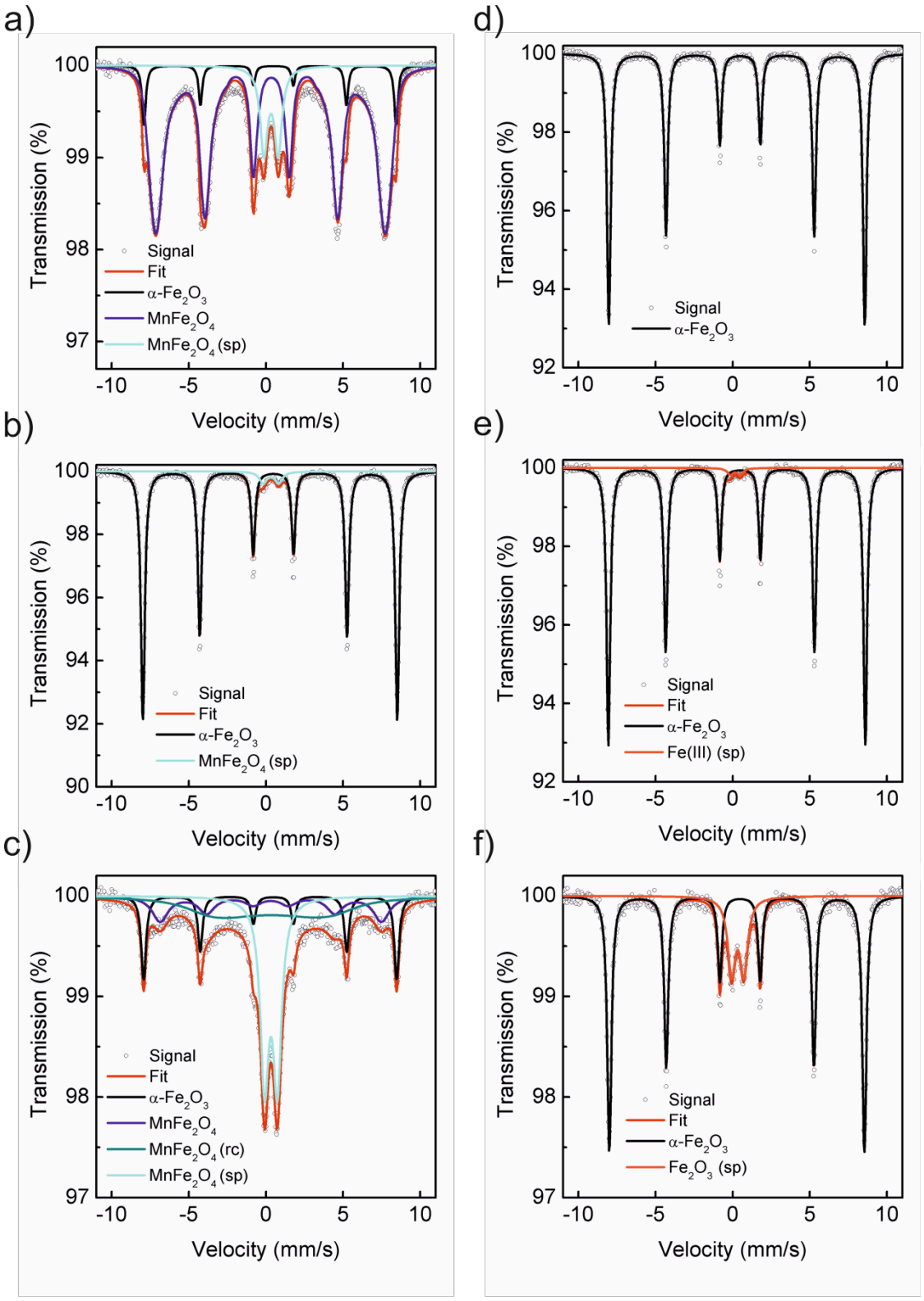

Hydroxylation
P 252 Monohydroxy CBZ
Hydroxylation
Amine
Hydrogen
abstraction
Dihydroxy CBZ
Decarboxylation
Further degradation
P179 Acridine

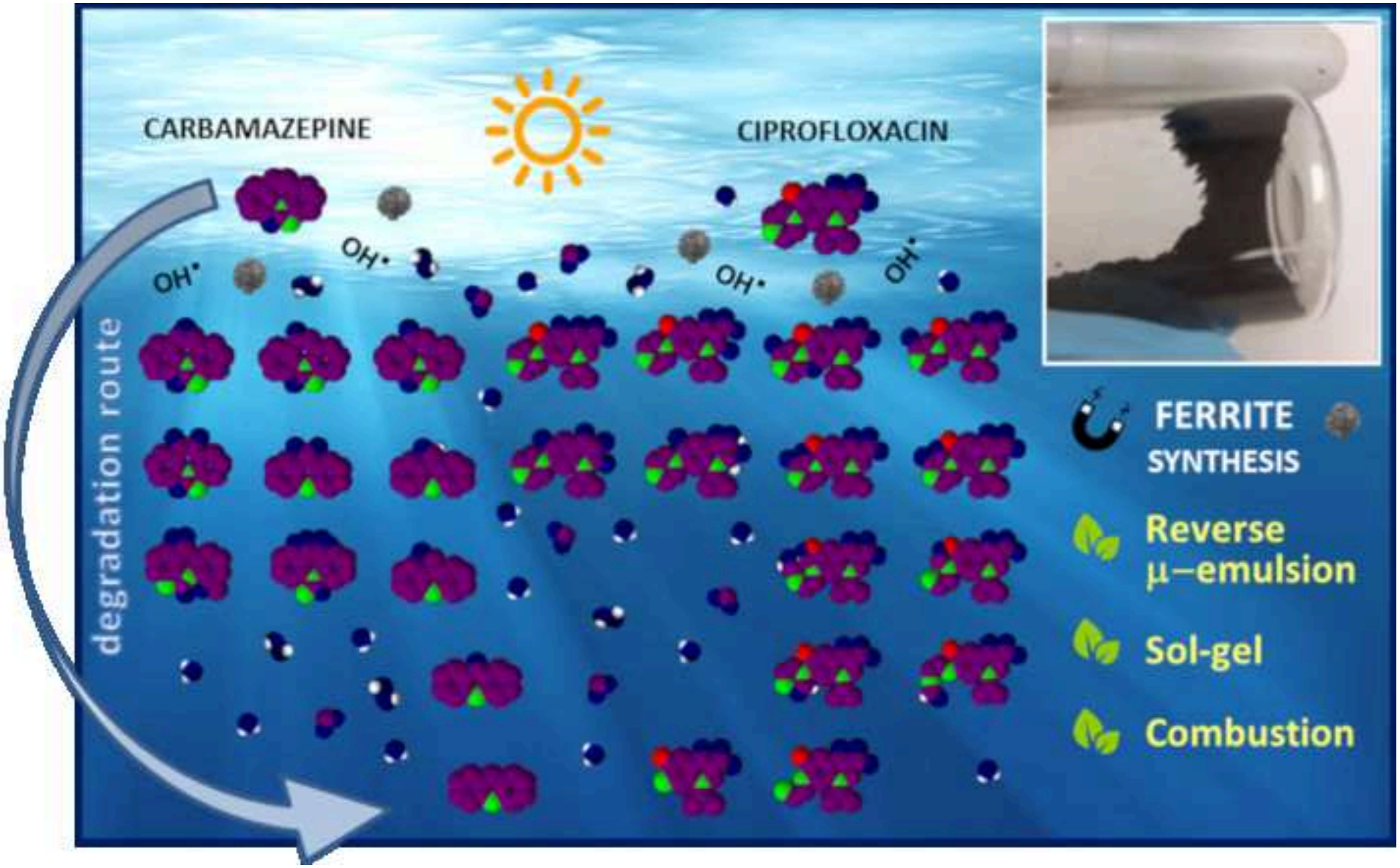
FIGURE SI1


a)
Transmission (%)
Velocity (mm/s)
Signal
Fit
α-Fe2O3
MnFe2O4
MnFe2O4 (sp)
b)
Transmission (%)
Velocity (mm/s)
Signal
Fit
α-Fe2O3
MnFe2O4 (sp)
c)
Transmission (%)
Velocity (mm/s)
Signal
Fit
α-Fe2O3
MnFe2O4
MnFe2O4 (rc)
MnFe2O4 (sp)
d)
Transmission (%)
Velocity (mm/s)
Signal
α-Fe2O3
e)
Transmission (%)
Velocity (mm/s)
Signal
Fit
α-Fe2O3
Fe(III) (sp)
f)
Transmission (%)
Velocity (mm/s)
Signal
Fit
α-Fe2O3
Fe2O3 (sp)

Highlights

- Magnetic ferrite catalysts were synthetized by new environmentally friendly methods.
- Ciprofloxacin and carbamazepine were effectively treated by solar photocatalysis.
- The sol-gel synthesized ferrite was more magnetic and more suitable for its reuse.
- The degradation pathways of ciprofloxacin and carbamazepine were elucidated.

Graphical Abstract



Novelty Statement

This piece of research includes the clean manufacturing of novel magnetically recoverable water treatment ferrite-catalysts synthesized by three environmentally-friendly designed preparation methods, replacing toxic chemicals of conventional synthesis methods by harmless ones. These catalysts were applied in the effective photo-Fenton treatment of ciprofloxacin and carbamazepine, two pharmaceuticals frequently present in natural water bodies which degradation routes were investigated and postulated. All these are novel contributions to existing literature and are included within the scope of JHM, which specifically covers the ways of mitigating the risks that environmental pollutants pose to the environment, including the design and of application AOPs.



https://dspace.org/

Environmentally friendly synthesized and magnetically recoverable designed ferrite photo-catalysts for wastewater treatment applications

Hermosilla, Daphne; Han, Changseok; Nadagouda, Mallikarjuna; Machala, Libor; Gascó, Antonio ...

2019-09-10
Elsevier
https://doi.org/10.1016/j.jhazmat.2019.121200
Hermosilla D, Han C, Nadagouda M, et al., (2020) Environmentally friendly synthesized and magnetically recoverable designed ferrite photo-catalysts for wastewater treatment applications. Journal of Hazardous Materials, Volume 381, January 2020, Article number 121200

Downloaded from a DSpace repository. https://dspace.org/